SANDIA REPORT
SAND2006-5668
Unlimited Release
Printed September 2006

Report on ASC Project Degradation of Organic Materials

Joanne Budzien, David Chi S. Lo, John G. Curro, Aidan P. Thompson, Gary S. Grest, and Dana Rottach

Prepared by
Sandia National Laboratories
Albuquerque, New Mexico 87185 and Livermore, California 94550

Sandia is a multiprogram laboratory operated by Sandia Corporation,
a Lockheed Martin Company, for the United States Department of Energy's
National Nuclear Security Administration under Contract DE-AC04-94AL85000.

Issued by Sandia National Laboratories, operated for the United States Department of Energy by Sandia Corporation.

Available to DOE and DOE contractors from
U.S. Department of Energy
Office of Scientific and Technical Information
P.O. Box 62
Oak Ridge, TN 37831

Telephone: (865) 576-8401
Facsimile: (865) 576-5728
E-Mail: reports@adonis.osti.gov
Online ordering: http://www.osti.gov/bridge

Available to the public from
U.S. Department of Commerce
National Technical Information Service
5285 Port Royal Rd.
Springfield, VA 22161

Telephone: (800) 553-6847
Facsimile: (703) 605-6900
E-Mail: orders@ntis.fedworld.gov
Online order: http://www.ntis.gov/help/ordermethods.asp?loc=7-4-0#online

SAND2006-5668
Unlimited Release
Printed September 2006

Report on ASC Project Degradation of Organic Materials

Joanne Budzien
Computational Materials Science and Engineering

David Chi S. Lo
Material Mechanics

John G. Curro
Ceramic Processing and Inorganic Materials

Aidan P. Thompson
Multiscale Computational Material Methods

Gary S. Grest
Surface and Interface Sciences

Sandia National Laboratories
P.O. Box 5800
Albuquerque, New Mexico 87185-MS1411

Dana Rottach
Department of Chemical and Nuclear Engineering
University of New Mexico
Albuquerque, NM 87106

Abstract

Using molecular dynamics simulations, a constitutive model for the chemical aging of polymer networks was developed. This model incorporates the effects on the stress from the chemical crosslinks and the physical entanglements. The independent network hypothesis has been modified to account for the stress transfer between networks due to crosslinking and scission in strained states. This model was implemented in the finite element code Adagio and validated through comparison with experiment. Stress relaxation data was used to deduce crosslinking history and the resulting history was used to predict permanent set. The permanent set predictions agree quantitatively with experiment.

ACKNOWLEDGMENTS

Dan Hammerand provided advice and guidance on implementing the material model into Adagio, using the Fortran interface and the augmented Lagrangian wrapper.

Ben Spencer provided guidance and support for numerical issues related to performing computations to compare with experimental data.

CONTENTS

FIGURES

TABLES

LIST OF SYMBOLS

A	elastic modulus due to slip-tube entanglements
c	monomer density
c_{jk}	coefficients for a power series representation of the strain energy in terms of strain invariants
f	deformation scaling under uniaxial conditions for the entanglements from the slip-tube model
F	free energy
F_e	normalized force for the entanglement contribution
F_{ph}	free energy of the phantom model
F_0	original force measurement
F^{cont}	continuous force measurement
F^{int}	intermittent force measurement
G	shear modulus
G_c	chemical contribution to the shear modulus
G_e	entanglement contribution to the shear modulus
G_N^0	plateau modulus
G_x	modulus due to stage x crosslinking
G_x^{eff}	effective modulus attributed to stage x crosslinking
G_x^*	maximum modulus due to stage x crosslinking
G_2^{α}	modulus from stage two crosslinks that can contribute to stress transfer
G_2^{β}	modulus from stage two crosslinks that will not contribute to stress transfer
g_{α}	scaling parameter for the slip-tube in the α direction
H	parameter for bonded interactions
I_1	first strain invariant ($I_1 = \lambda_1^2 + \lambda_2^2 + \lambda_3^2$)
I_2	second strain invariant ($I_2 = \lambda_1^2\lambda_2^2 + \lambda_1^2\lambda_3^2 + \lambda_2^2\lambda_3^2$)
I_3	third strain invariant ($I_3 = \lambda_1^2\lambda_2^2\lambda_3^2$)
k	rate constant for scission
k_B	Boltzmann's constant
L	slip-tube parameter
L_i	length in the i direction
L_{i0}	original length in the i direction
m	mass of a simulation site

N	(1) number of terms in the Ogden form of the strain energy (2) slip-tube parameter
N_e	entanglement spacing
p	indeterminate Lagrangian multiplier
PS	permanent set
r	distance between simulation sites
R_0	maximum bond length
S	$S = g_1 + g_2 + g_3 - 3$
t	time
T	temperature
W	strain energy
U_b	potential energy due to bonded interactions
U_{ev}	potential energy due to excluded volume
α_p	p^{th} term for the exponent for the Ogden form of the strain energy
$\Delta\lambda$	small changes in deformation
ε_{LJ}	Lennard-Jones energy parameter
λ	current sample deformation
λ_s	deformation corresponding to the system state of ease
λ_x	(1) under uniaxial deformation, the deformation at which the stage x crosslinks were introduced. (2) for arbitrary deformation, the principal stretch ratio in direction x
Λ	Lagrangian multiplier
μ_p	p^{th} term for the material modulus for the Ogden form of the strain energy
ν	actual total strand density
ν_{gel}	strand density required for gelation (stage one strand densities do not include this value)
ν_x	actual strand density remaining from crosslinking at stage x
ν_x^*	maximum actual strand density for stage x
ν_x^{eff}	effective strand density for stage x
ρ	number density
σ_i	Cauchy stress in the i direction
σ_{LJ}	Lennard-Jones length parameter
τ	Lennard-Jones time unit
ϕ	crosslink functionality
Φ	stress transfer function

1. INTRODUCTION

Chemical aging of rubber under strain can be a problem for seals and o-rings left in service for years. Two related phenomena are observed experimentally: 1) stress relaxation in the rubber component with time and 2) permanent set (failure of the rubber component to return to the original dimensions upon removal of the strain). Both of these phenomena indicate a reduction in sealing force, which means that after years in service a rubber seal or o-ring no longer performs its desired function. While both physical and chemical processes contribute to the observed stress relaxation[1,2], failure of the o-ring is due to chemical aging. Previous work used an elastic material model to give an analytical solution for the stress in an o-ring[3]. The goal of this project is to predict stress relaxation and permanent set due to chemical changes in the polymer network that make up the rubber.

The technical difficulty in making these predictions lies in the multiscale nature of the problem. Any single chemical reaction is fast (on the order of femtoseconds) and involves only a few atoms. However, chemical reactions change the network that gives the rubber its elastic nature. The cumulative effect of these small changes can be quite large as seen in field-aged o-rings with permanent sets of 30 to 60% after 16 to 22 years in service[4].

Therefore, the challenge is to develop a model that includes the molecular details of chemical changes of the network topology, yet can make predictions of the long-time behavior. We accomplished this through a hierarchical approach. First, we smeared out the specific chemical details. The polymer chains used in molecular dynamics simulations include bonded connectivity and excluded volume, but individual sites correspond to a length scale of several mers, not simply a single atom or small chemical group. Coarse-graining in this manner allows us to investigate the physics of the sample stress with changes in network topology, using simulations that require days rather than months on high-performance computers. In this first phase of model development, the detailed kinetics of the reactions are unimportant; what matters is how the relative level of crosslinking changes over time coupled with the strain history of the sample.

Simulations were performed with crosslinking of an original network in an unstrained state (stage 1). The sample was strained and a second phase of crosslinking was done in the strained state (stage 2). Determining the zero stress deformation allows the permanent set to be calculated. We can then compare the simulated results with predictions from rubber elasticity models suggested in the literature. Doing this permits a more rigorous test of the rubber elasticity models than simply requiring the stress to match. Scission of the original network (stage 3) and monitoring of the resulting stress change yields information about the coupling of reaction and strain history. Complete scission of the original network does not negate its effect on the material properties. Instead, the bias in the reactions available to the second network causes a memory effect so that, for all practical purposes, a fraction of the second network acts as though it were the original network. We have quantified this fraction through stress transfer functions.

The outcome of this procedure was a constitutive model connecting changes in the microscopic network topology during a strain history with the macroscopic stress. This model was implemented into the material library Strumento that is used in conjunction with the finite element code Adagio. This report provides details about the new constitutive model and key points about how this model can be used to perform finite element calculations. The remainder of this introduction is a brief overview of rubber elasticity from both the atomistic and continuum viewpoints. The following section describes features of the molecular dynamics simulations with emphasis on the specific simulation features that were required to develop the constitutive model. Later sections of this report describe particular features of the model as implemented in Adagio/Strumento. The final section of the main body is a comparison of finite element calculations and experimental data. Appendix A is a condensed version of the material model and instructions on use for finite element calculations. The Fortran code used to generate the scaling factors for the slip-tube model is also included in this report as Appendix B. This is the final report. Details of the stress transfer function, particularly the extension to multiple stages of crosslinking and scission, and some simulation results were given in the previous report[5] and are not repeated here.

1.1. Rubber Elasticity (from the atomistic viewpoint)

Rubber elasticity is primarily the result of entropy. Polymer molecules have maximum entropy in a random coil conformation. Crosslinking the polymer molecules into a network restricts the conformations that they can adopt. Straining the network further restricts the conformations that the strands can adopt. Physically, the measured stress arises from the strands pulling or pushing to achieve an equilibrium conformation, with entropy maximization as the driving force. The stress can be calculated from the difference in free energy between the deformation at which the network was formed and the imposed deformation. Networks exhibit zero stress in the deformation at which they were formed. This deformation is termed the state of ease.

Strands that are between two crosslinks contribute to the measured stress. Dangling ends do not because they can adopt the entropically favored random coil conformations. Loops (a strand that is terminated at both ends by the same crosslink) do not unless the loop forms a knot with another restricted strand. This intertwining will support stress because it also provides a physical restriction on the conformations that the polymer strands can adopt. Thus, crosslinking a system of long polymer chains will not only give a network based on the chemical connectivity of the strands, but also have some stress supported by trapped entanglements (physical snarls of strands that cannot unravel because of the network structure).

Referring back to the chemical aging problem, two processes occur in rubber networks held in a strained state: chemical crosslinking of a new network with its state of ease in the strained state and scission of both networks. The independent network hypothesis (originally proposed by Tobolsky and coworkers[6]) states that the overall stress in the sample can be considered as the sum of the stresses in each network individually. Since networks in their state of ease should have zero stress contribution, simply adding more

crosslinks at a given deformation should have no effect on the stress. Previous simulations[7] showed this to be true in uniaxial extension and this holds true also in uniaxial compression (see Figure 1.1).

The phenomenon of permanent set arises because these two networks have competing effects on the overall sample stress. The state of ease of the sample will be a deformation intermediate between the deformations at which the two networks were crosslinked. The amount of permanent set observed will depend on the relative amounts of the networks. Heavily crosslinked networks will pull more strongly than lightly crosslinked networks. Networks crosslinked to the same extent will not necessarily exhibit the same stress because of the trapped entanglements. Only the first crosslinking about the gel point traps entanglements; later stages of crosslinking do not trap additional entanglements.

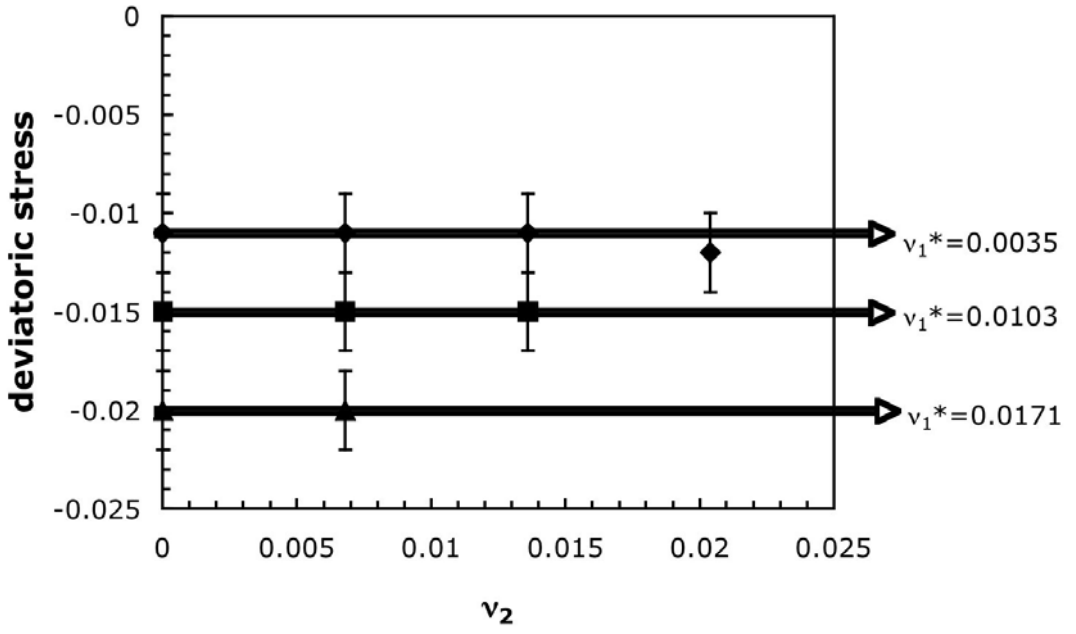

Figure 1.1: Illustration of the Independent Network Hypothesis
These systems were crosslinked at λ_1=1.0, compressed to λ_2=0.534, and then reacted to a second stage chain density of ν_2. ν_1* is defined as chain density above the gel point (ν_{gel}=0.0033). Error bars are standard deviation in deviatoric stress values during production time. Simulation details are given in Section 2: Molecular Dynamics Simulations. Units are reduced Lennard-Jones units.

The effect of network scission on the stress is not as straightforward because of the coupling of reaction and strain histories. Figure 1.2 shows a schematic of the sequential crosslinking and scission for two networks. While the two networks are independent if only crosslinking occurs, scission of the original network does not negate its effect. The sample retains a memory of the original network because of its influence on how the second network formed. The first network was free to react in any chemically feasible manner. The second network was limited to reactions that could find each other under the restrictions imposed by the first network. Thus, as seen in the second panel of Figure 1.2, the reactions to create the second network occur only between strands in close proximity under the restraints imposed by the first network. Therefore, when the first network

scissions, not all of the stress is released. Some fraction of the second network may act like crosslinks from the original network and continue to support stress. This effect is probably not a one-for-one exchange, but is more likely to be the collective effect of several crosslinks. This memory effect (the second network effectively acting as the first network) can be quantified by stress transfer functions. The incorporation of stress transfer functions into a constitutive model for the chemical aging of rubber under strain is the main technical advance of this work.

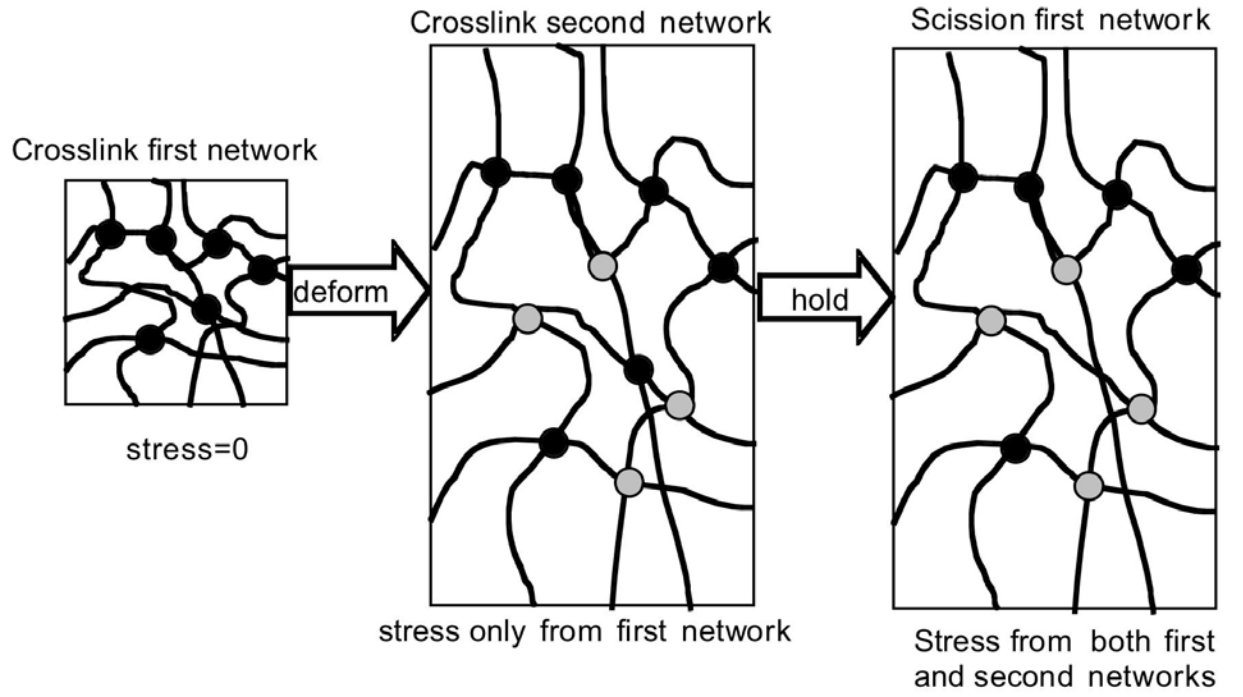

Figure 1.2: Schematic of Coupling Strain and Reaction Histories

1.2. Rubber Elasticity (from the continuum viewpoint)

At the continuum level, rubber elasticity is described in constitutive equations relating stress to strain, just like in standard elasticity theory. For the simple case of one network (i.e., no chemistry occurs in the strained state), the stress is generally written in terms of principal stretch ratios $\{\lambda_i\}$ or, frequently, combinations of the principal stretch ratios, which are invariant under rotation. The standard way to write the three strain invariants is

$$I_1 = \lambda_1^2 + \lambda_2^2 + \lambda_3^2$$
$$I_2 = \lambda_1^2\lambda_2^2 + \lambda_1^2\lambda_3^2 + \lambda_2^2\lambda_3^2$$
$$I_3 = \lambda_1^2\lambda_2^2\lambda_3^2 \quad (1)$$

At room temperature, most rubber samples are nearly incompressible with a Poisson's ratio of about 0.5. Incompressibility leads to the third strain invariant (I_3) being unity.

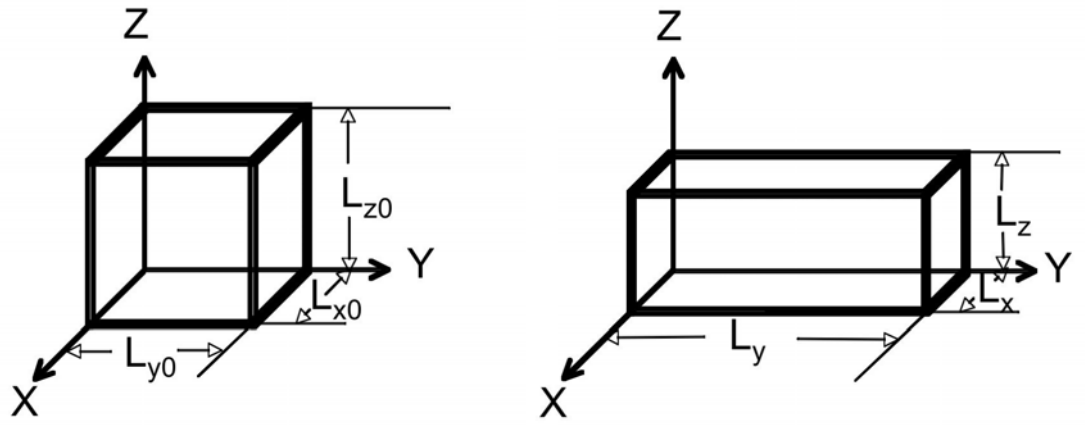

$$\lambda_x = \frac{L_x}{L_{x0}} \quad \lambda_y = \frac{L_y}{L_{y0}} \quad \lambda_z = \frac{L_z}{L_{z0}}$$

Figure 1.3: Illustration of Principal Stretch Ratios in Cartesian Coordinates

Many theories of rubber elasticity can be written as special cases of incompressible hyperelasticity theory. The principal Cauchy stresses $\{\sigma_i\}$ can be calculated as derivatives of the strain energy (W)

$$\sigma_i = \lambda_i \frac{\partial W}{\partial \lambda_i} - p \tag{2}$$

where p is an indeterminate Lagrangian multiplier dependent on the boundary conditions of the specific problem. The strain energy for an incompressible hyperelastic material (the ideal rubber) can be written as

$$W = \sum_{j=0}^{\infty}\sum_{k=0}^{\infty} c_{jk}(I_1 - 3)^j (I_2 - 3)^k \tag{3}$$

where the c_{jk} are particular to the model chosen and physical system under study.

The classical theories of rubber elasticity for the affine[8] and phantom[9,10] networks can be written as the first term of the first strain invariant:

$$W = \frac{G}{2}(I_1 - 3) \tag{4}$$

The difference between these models is relating the modulus G to the molecular details of the systems. The phantom model has a modulus that is one-half the value of the affine model. Many people have worked on modifications of this general formula to account for the molecular details of imperfections in the networks, but most of that work is relating G to the molecular network.

The Mooney-Rivlin equation[11,12] may be written as

$$W = c_{10}(I_1 - 3) + c_{01}(I_2 - 3) \tag{5}$$

While this general form is often used to describe experimental data under moderate strains, efforts to connect the constants c_{10} and c_{01} to molecular quantities have been much less successful.

Another general power series for the strain energy for an incompressible, hyperelastic material in terms of principal stretches is attributed to Ogden[13]

$$W = \sum_{p=1}^{N} \frac{\mu_p}{\alpha_p} \left(\lambda_1^{\alpha_p} + \lambda_2^{\alpha_p} + \lambda_3^{\alpha_p} - 3 \right)$$

(6)

where N, μ_p, and α_p are all material dependent. The affine, phantom, and Mooney-Rivlin equations can also be written as special cases of this equation.

The difficulty in developing a constitutive model for rubber elasticity is relating the molecular network and changes therein to the macroscopic properties. Until recently, approaches from the molecular and continuum viewpoints were too widely separated to connect. The new connection method is simulation. With the advances in simulation techniques, particularly parallelization that allows much larger systems to be simulated, polymer networks can now be studied computationally. Simulation provides the ability to calculate stress and to know all the topological information of the network. Even more appealing, complete control over the deformation and chemical changes to the network is possible.

2. MOLECULAR DYNAMICS SIMULATIONS

The purpose of performing molecular dynamics simulations was to evaluate standard constitutive models for their general physics. Our goal was to find a constitutive model appropriate for use with the independent network hypothesis that predicts permanent set. Permanent set is measured in field experiments and is related to sealing force. Here, permanent set is used as a more rigorous criterion than simply predicting stress. Using the assumption that the moduli can be used as adjustable parameters, all standard models of rubber elasticity have had some success in fitting experimental stress. The compatibility with the independent network hypothesis is important because of the stress transfer during scission. We want to keep the form of the constitutive model constant during chemical reaction and use effective crosslink densities (crosslink densities modified by the stress transfer function) to calculate stress and permanent set.

2.1. General Model

We performed molecular dynamics simulations of coarse-grained polymer models. This reduces the simulation time by ignoring the fine chemical detail of polymer systems. However, the essential physics of rubber elasticity are retained. Each polymer molecule starts as a linear chain of 500 sites. These chains cannot cross each other or otherwise overlap in an unphysical manner. Reactions are performed on the linear chains to link them into networks. In this way, the effect of crosslinking and the resultant trapping of entanglements can be investigated in general for any rubber network system.

The polymer chains follow a standard bead-spring model[14] with an excluded volume interaction of

$$U_{ev}(r) = 4\varepsilon_{LJ}\left[\left(\frac{\sigma_{LJ}}{r}\right)^{12} - \left(\frac{\sigma_{LJ}}{r}\right)^{6} + \frac{1}{4}\right] \qquad r \le 2^{1/6}\sigma_{LJ}$$

$$U_{ev}(r) = 0 \qquad r > 2^{1/6}\sigma_{LJ}$$

(7)

For this work, both ε_{LJ} and σ_{LJ} were set to unity. Time is in reduced units of $\tau = \sigma_{LJ}\sqrt{m/\varepsilon_{LJ}}$ with m also set to unity. In addition, adjacent sites are connected by finitely extensible non-linear elastic (FENE) bonds of the form

$$U_b(r) = -\frac{HR_0^2}{2}\ln\left[1 - \left(\frac{r}{R_0}\right)^2\right] \qquad r \le R_0$$

$$U_b(r) = \infty \qquad r > R_0$$

(8)

with $H=30\varepsilon_{LJ}/\sigma_{LJ}^2$ and $R_0=1.5\sigma_{LJ}$. Crosslinks use the same bonding potential; the difference is that sites involved in a crosslink have three bonded neighbors instead of only

two. This results in tetrafunctional crosslinks (four strands emanate from the pair of sites forming the extra bond).

All simulations were performed using the LAMMPS99 code[15] modified to perform reactions[16]. The integration method was a velocity Verlet algorithm under NVT ($T^*=1.0$, $\rho^*=0.85$) conditions with a Nose-Hoover thermostat. The time step was 0.005 or 0.01 τ. Systems began as 500 linear chains with 500 sites each. On each chain, twenty sites are chosen randomly as reactive (i.e., capable of forming three bonds instead of the standard two bonds). These reactive sites are chosen under the rules that 1) no chain ends are designated reactive and 2) reactive sites on the same chain must be separated by at least two bonds. Reactions are probabilistic. At regular intervals, the distance between reactive sites is calculated and compared to a capture radius (typically between 1.122 and 1.3 σ_{LJ}). Pairs of reactive sites within the capture radius then form a bond with some reaction probability (which was adjusted to keep quasi-equilibrium conditions). In the unstrained state, crosslinking 20, 40, or 60% of the reactive sites formed the original, stage 1 networks.

The systems were then uniaxially deformed in a series of affine steps, keeping the volume constant. The coordinates for each site were scaled as $\Delta\lambda x$, $y/\sqrt{\Delta\lambda}$, and $z/\sqrt{\Delta\lambda}$ with typical values of $\Delta\lambda$=0.01. The molecular dynamics simulation continued through this deformation. Consequently, while each step is affine, the system adjusts through the entire deformation, resulting in an overall nonaffine process.

After equilibration at the new deformation (designated λ_2), a second stage of crosslinking occurred. Again, the levels of crosslinking are 20, 40, and 60% of the starting reactive sites with the limitation that a maximum of 80% of the starting reactive sites are used in a given system. With two networks, a state of ease between the two deformations is possible and a permanent set can be observed. Performing simulations at deformations between the two crosslinking deformations permits the determination of λ_s (the deformation corresponding to the system state of ease) and, thus, calculation of the permanent set from

$$PS = \frac{\lambda_s - 1}{\lambda_2 - 1} * 100 \quad (9)$$

2.2. Permanent Set from Uniaxial Extension Results

For the uniaxial extension case, the systems were deformed to a stretch ratio of λ_2=2.0. These results were published in the journal Macromolecules[17]. Four standard models of rubber elasticity were compared to the simulated permanent set results: phantom[9,10], affine[8], constrained junction[18], and slip tube[19]. The phantom and affine models differ only by a multiplicative constant. Therefore, they both predict the same result: the permanent set depends only on the relative degree of crosslinking of the two systems. The constrained junction model is a modification of the affine model to account for the effect of entanglements. It also predicts that permanent set is only a single-valued function of the ratio of crosslinking in stage 2 to that of stage 1. As seen in Figure 2.1, initial crosslinking density is important for the simulation results. The three different levels of stage one crosslink density give rise to three discrete series of permanent set results.

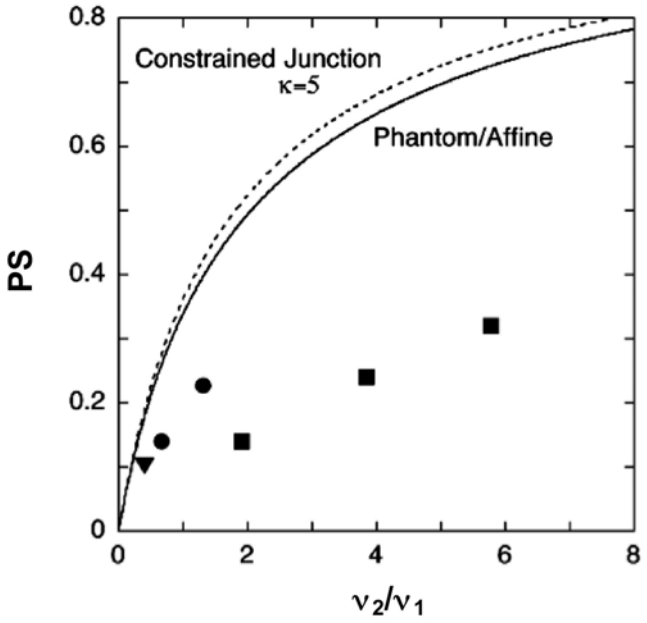

Figure 2.1: Permanent Set. Comparison of Simulated Results and Classical Rubber Elasticity Theories Predictions.

Symbols are simulated results for a double network in uniaxial extension. Squares are 20% initial crosslinking, circles are 40% initial crosslinking, and the triangle is 60% initial crosslinking.

While the slip-tube model is a modification to the phantom model that incorporates the effect of entanglements, the slip-tube model predicts that both initial extent of crosslinking and the relative degrees of crosslinking matter. As shown in Figure 2.2, the slip-tube model is in good agreement with the simulation results. Therefore, the slip-tube model is chosen as the constitutive model to be implemented in the finite element code. The slip-tube model is described in detail in the next chapter.

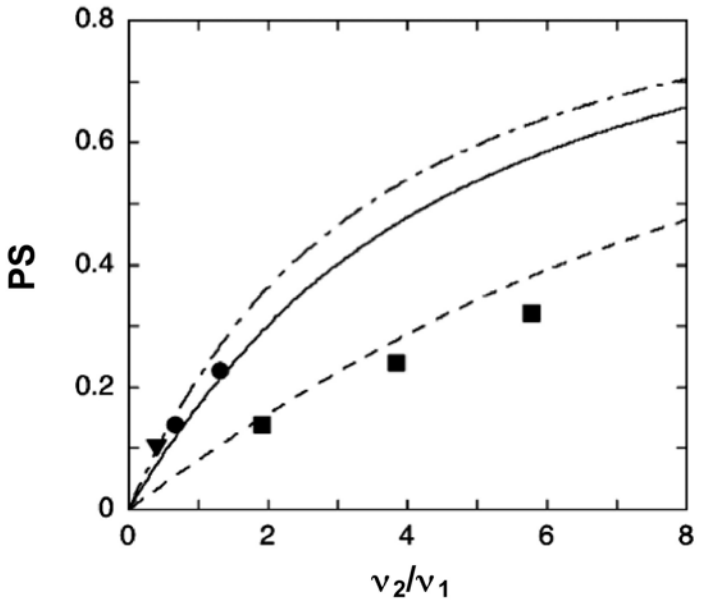

Figure 2.2: Permanent Set. Comparison of Uniaxially Extended Simulations to the Slip-Tube Model.
Symbols are simulated results. Squares are 20% initial crosslinking, circles are 40% initial crosslinking, and the triangle is 60% initial crosslinking.

2.3. Model-free Determination of the Stress Transfer Function from Simulation

The stress transfer functions are only available for systems undergoing scission. Using the double network systems (still at the stage two deformation), crosslinks were removed from the original network. For convenience, the maximum removal of stage one crosslinks is to the gel point. This situation keeps the entanglements trapped with the same state of ease, but the stress from the stage one chemical crosslinks is zero.

The model-free approach uses the intuitive definition of effective chain density. What single stage network at this strain would have the same stress as the double network after scission has? The stresses for each of the initial chain densities at the second stage strain was recorded and plotted as a function of stage one chain density. As Figure 2.3 shows, deviatoric stress is linearly related to the original chain density. Consequently, determining the effective chain density simply requires reading the ν_1 value from Figure 2.3 at the appropriate stress. The stress transfer function (Φ) is related to the chain densities through

$$\nu_1^{eff} = \nu_1 + \Phi \nu_2$$
(10)

where ν_1 is actual density of stage one chains (only counting chains above the gel point), ν_2 is the actual density of stage two chains, and ν_1^{eff} is the effective density of stage one chains. In these simulated systems, ν_1 and ν_2 are known and ν_1^{eff} is determined from Figure 2.3, which allows Φ to be determined by simple algebra. Results of this model-free determination of the stress transfer function are shown in Figure 2.4.

To be of value in the finite element code, the stress transfer function needs to be calculable from the chain densities without needing the stress. Based on theoretical considerations for the phantom model, Fricker[20] proposed that the stress transfer function for a two-stage network has the analytical form

$$\Phi = \frac{\nu_1^* - \nu_1}{\nu_1^* + \nu_2} = 1 - \frac{\nu_1 + \nu_2}{\nu_1^* + \nu_2}$$
(11)

where ν_1* denotes stage one chain density (above the gel point) before scission, ν_1 denotes stage one chain density (above the gel point) after scission, and ν_2 denotes stage two chain density. Figure 2.4 shows that this equation is a good approximation to the simulation results. An extension of this formula for multiple stages of crosslinking and scission was implemented in the material model and is given in Appendix A: Summary of Material Model.

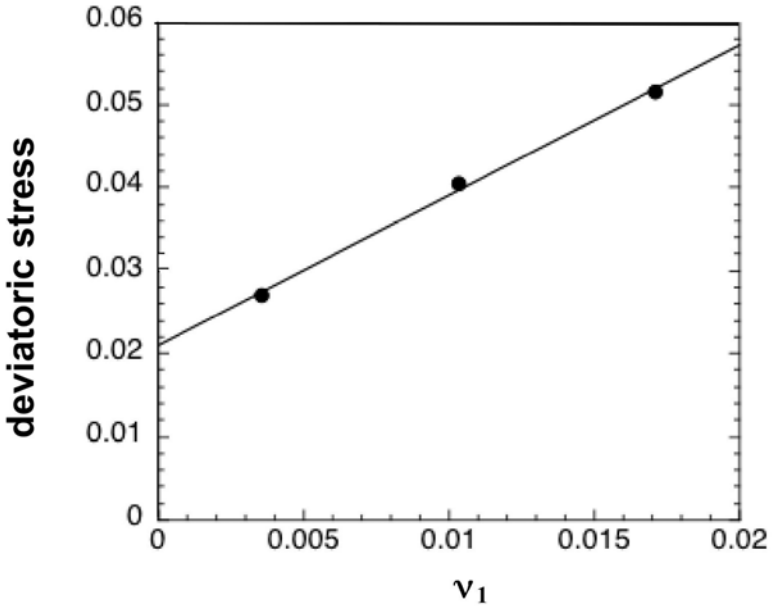

Figure 2.3: Deviatoric Stress for Single-Stage Network Stretched to λ_2=2.0
Note that ν_1 includes only stage one chains above the gel point. Points are simulation results; line is a linear fit to the simulation results.

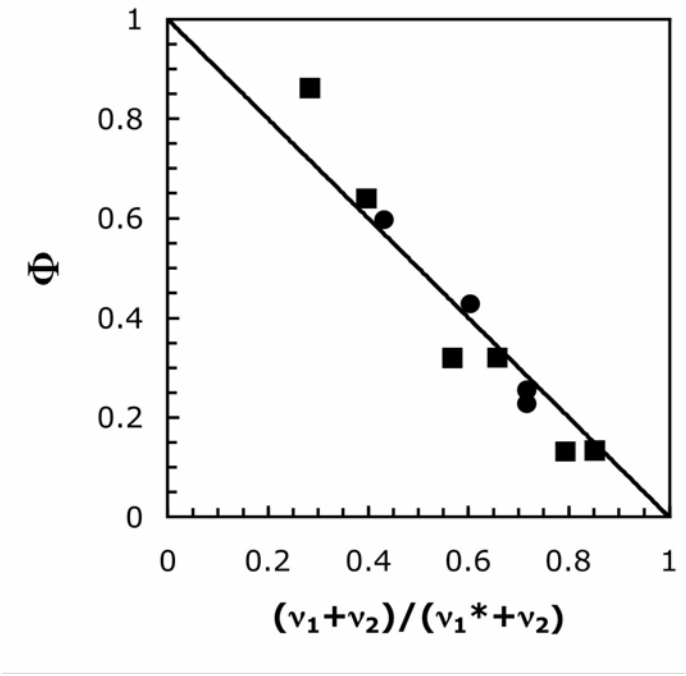

Figure 2.4: Stress Transfer Functions. Comparing Model-Free Value with the Fricker[20] Function.

Circles denote removal of stage one crosslinks to the gel point; squares denote systems with remaining stage one crosslinks above the gel point. The line is Fricker's analytical expression from Eq. 11.

2.4. Uniaxial Compression Results

For the uniaxial compression case, the systems were deformed to a stretch ratio of λ_2=0.534. Permanent set was also calculated for double networks with the second stage crosslinked in compression (shown in Figure 2.5). Similar to the extension results, the three original crosslinking densities give rise to three series of permanent set data. The slip-tube model predictions are also presented in Figure 2.5 with good agreement between theory and simulation.

We know that stress transfer is important during scission at λ_2. However, does that stress transfer effect (a portion of the stage two network acting as stage one networks) carry over for scission that occurs in other deformations? In other words, will the stage two network always "come to the rescue" of the stage one network or is that an artifact of the removal of crosslinks at λ_2? As a test, the stress was measured for three cases. For case 1, after crosslinking in the compressed state, the double network was stretched back to λ=1.0, allowed to equilibrate, and the stress was measured. Case 2 began from the end of the case 1 equilibrated system and had stage one crosslinks removed to the gel point. The system was reequilibrated and stress was then measured. Case 3 began with the double network just after crosslinking in the compressed state. The system was equilibrated, and then stage one crosslinks were removed to obtain the gel point concentration. The system was

then stretched to λ=1.0, equilibrated, and then the stress was measured. λ=1.0 was chosen so that only the effect of the stage two crosslinks is seen.

Figure 2.6 shows the stress of case 1 (double network only). As one would expect, the deviatoric stress clearly can be grouped according to level of stage two crosslinking. The networks subjected to scission are given in Figure 2.7. Within error, both treatments give the same stress; however, scission at $\lambda=\lambda_2$ generally gives a slightly higher stress, closer to the value of the double network without scission.

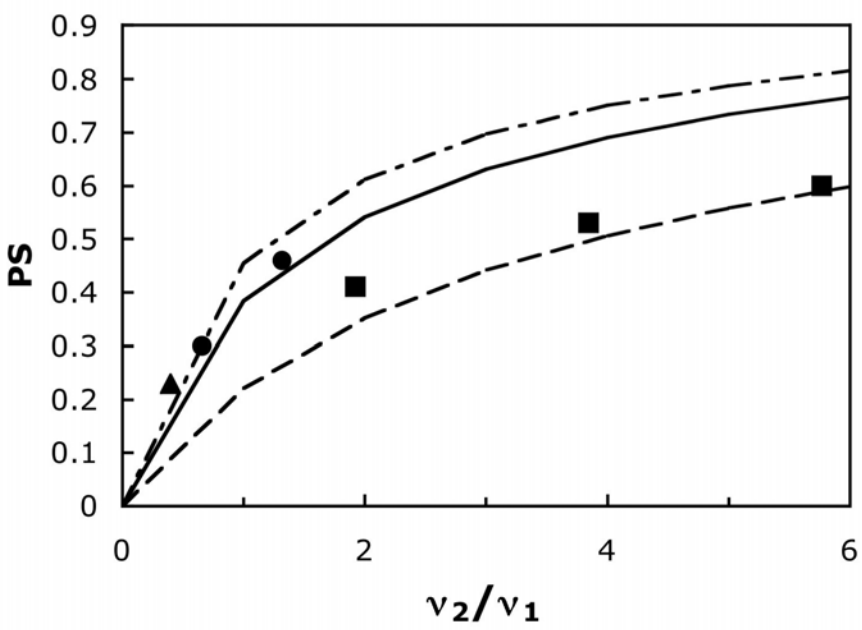

Figure 2.5: Permanent Set for Compressed Simulations Compared to Slip-Tube Model.

Symbols are simulated results. Squares are 20% initial crosslinking, circles are 40% initial crosslinking, and the triangle is 60% initial crosslinking. Lines are slip-tube model results.

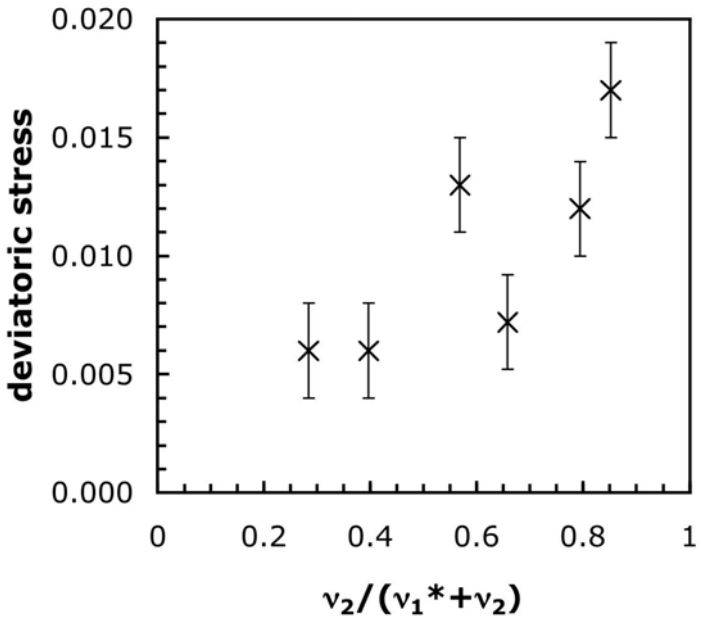

Figure 2.6: Stress from Double Network Crosslinked at λ_2=0.534 with Stress Measured at λ=1.0

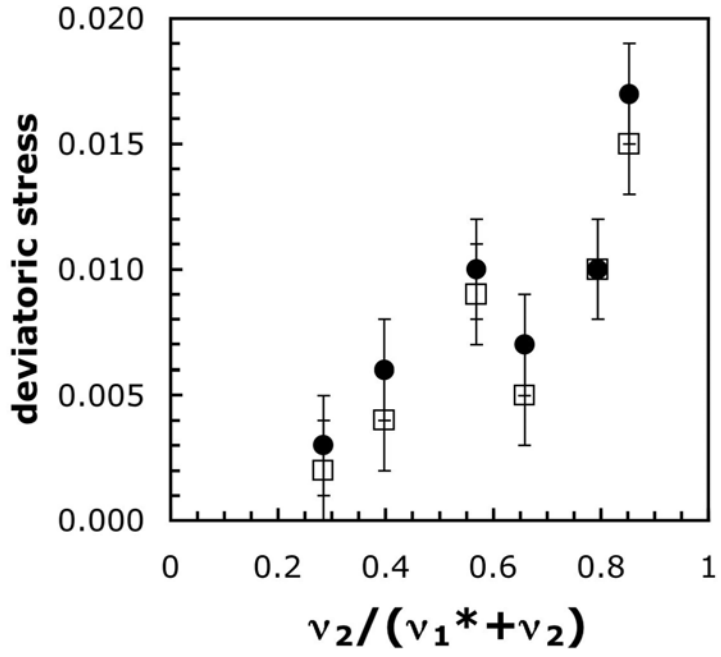

Figure 2.7: Stress from Double Networks Crosslinked in Compression and Stretched to λ=1.0. Does Deformation at Which Stage 1 Scission Occurs Have an Effect?

The squares are stage one crosslinks removed at λ_4=1.0. The circles are stage one crosslinks removed at λ_3=0.534. Stresses for systems are measured at λ=1.0.

3. THE SLIP-TUBE MODEL

Rubinstein and Panyukov[19] developed a tube model that includes the effect of entanglements as deformation is applied to a sample. This slip-tube model is in good agreement with the simulated permanent set results. Unfortunately, as originally formulated, the free energy calculation involves a self-consistent calculation at every deformation. This is computationally intensive and impractical for large systems using the finite element code. Instead, a deformation range suitable for o-rings has been identified and self-consistent calculations were done within that range. The resulting strain energy was fit analytically to a power series of strain invariants. The method used to determine that power series is given in the first section of this chapter along with the coefficients of that power series and figures illustrating goodness of fit. The second section of this chapter details the stress calculation implemented in the finite element code and shows a comparison of stress calculated from the finite element code with the original slip-tube model fit to experimental data.

3.1. Analytical Fit to the Strain Energy Equation

The free energy expression for the original formulation of the slip-tube model is[19]

$$F = \frac{A}{2}\sum_{\alpha}\left(\frac{\lambda_\alpha}{g_\alpha^{1/2}} + \frac{g_\alpha^{1/2}}{\lambda_\alpha}\right) - \frac{A}{3}\sum_{\alpha}\ln\left(\frac{N}{L}g_\alpha\right) + F_{ph} \quad (12)$$

where A is an elastic modulus due to the entanglements, λ_α is a principal stretch in the α direction, N and L deal with the tube, and F_{ph} is the free energy of the phantom chain model. The g_α are used to renormalize the deformation of the tube in a given direction. In an affine model, the microscopic deformation scales uniformly with the macroscopic deformation. In the slip-tube model, the microscopic deformation (denoted by prime) is

$$\lambda_\alpha' = \frac{\lambda_\alpha}{g_\alpha^{1/2}} \quad (13)$$

To calculate values for g_α, Eq. 12 must be minimized with respect to g_α under the condition that the sum of the three g_α equals three. Using a Langrangian multiplier method, the equations to solve are

$$\frac{12\Lambda}{A} = 3\left(-\frac{\lambda_2}{g_2^{3/2}} + \frac{1}{g_2^{1/2}\lambda_2}\right) - \frac{4}{g_2} \quad (14)$$

$$g_1^{3/2}\left[\frac{12\Lambda}{G_e}\lambda_1\right]-3g_1+4g_1^{1/2}\lambda_1+3\lambda_1^2=0$$
(15)
$$g_3^{3/2}\left[\frac{12\Lambda}{G_e}\lambda_3\right]-3g_3+4g_3^{1/2}\lambda_3+3\lambda_3^2=0$$
(16)
$$S=g_1+g_2+g_3-3$$
(17)

where Λ is the Lagrangian multiplier. From these equations, the set of $\{g_\alpha\}$ are a function of the set of $\{\lambda_\alpha\}$. Solving these equations for a general case is difficult. Instead, an iterative technique is used to solve these equations numerically at a specific deformation. The flow chart on the next page shows an outline of the steps. For Eqs. 15 and 16, a cubic equation[21] in $g_\alpha^{1/2}$ is solved and the root which is physical (i.e., positive and smaller than the square root of 3) is chosen. The use of a secant method[22] gives successively better approximations to $g_2^{1/2}$. Like all iterative techniques, a good initial guess is required to obtain reasonable solutions. The program used to calculate a set of $\{g_\alpha\}$ is given in Appendix B.

The next step is to calculate $\{g_\alpha\}$ for many sets of $\{\lambda_\alpha\}$. The overall goal is to have a strain energy function for arbitrary deformation (subject only to the limitation of an incompressible material). Strain energy for an arbitrary deformation[8] can be written as

$$W=\sum_{p,q=0}^{\infty}c_{pq}(I_1-3)^p(I_2-3)^q$$
(18)

where

$$I_1=\sum_{i=1}^{3}\lambda_i^2$$
(19)
$$I_2=\lambda_1^2\lambda_2^2+\lambda_2^2\lambda_3^2+\lambda_3^2\lambda_1^2$$
(20)
$$I_3=\lambda_1^2\lambda_2^2\lambda_3^2=1$$
(21)

c_{00} =0 so that zero deformation corresponds to zero strain energy. To match with the slip-tube strain energy, Eq. 12 is written as

$$\frac{W_{ST}}{A} = \frac{1}{2}\sum_{\alpha}\left(\frac{\lambda_\alpha}{g_\alpha^{1/2}} + \frac{g_\alpha^{1/2}}{\lambda_\alpha}\right) - \frac{2}{3}\sum_{\alpha}\ln\left(g_\alpha^{1/2}\right) - 3 \quad (22)$$

This function also goes to W=0 for $\{\lambda_\alpha\}$=1. The strain energies for many deformations corresponding to $0.3 \le \{\lambda_\alpha\} \le 3.0$ were calculated. This range was chosen as representative of the types of deformation encountered during standard O-ring usages. The deformations were chosen systematically by a double loop over λ_1 and λ_2 (each one taking values between 0.3 to 3.0) with $\lambda_3 = \frac{1}{\lambda_1\lambda_2}$ and keeping only the points such that all three principal stretch ratios lie between 0.3 and 3.0. Figure 3.2 shows the corresponding values of the strain invariants.

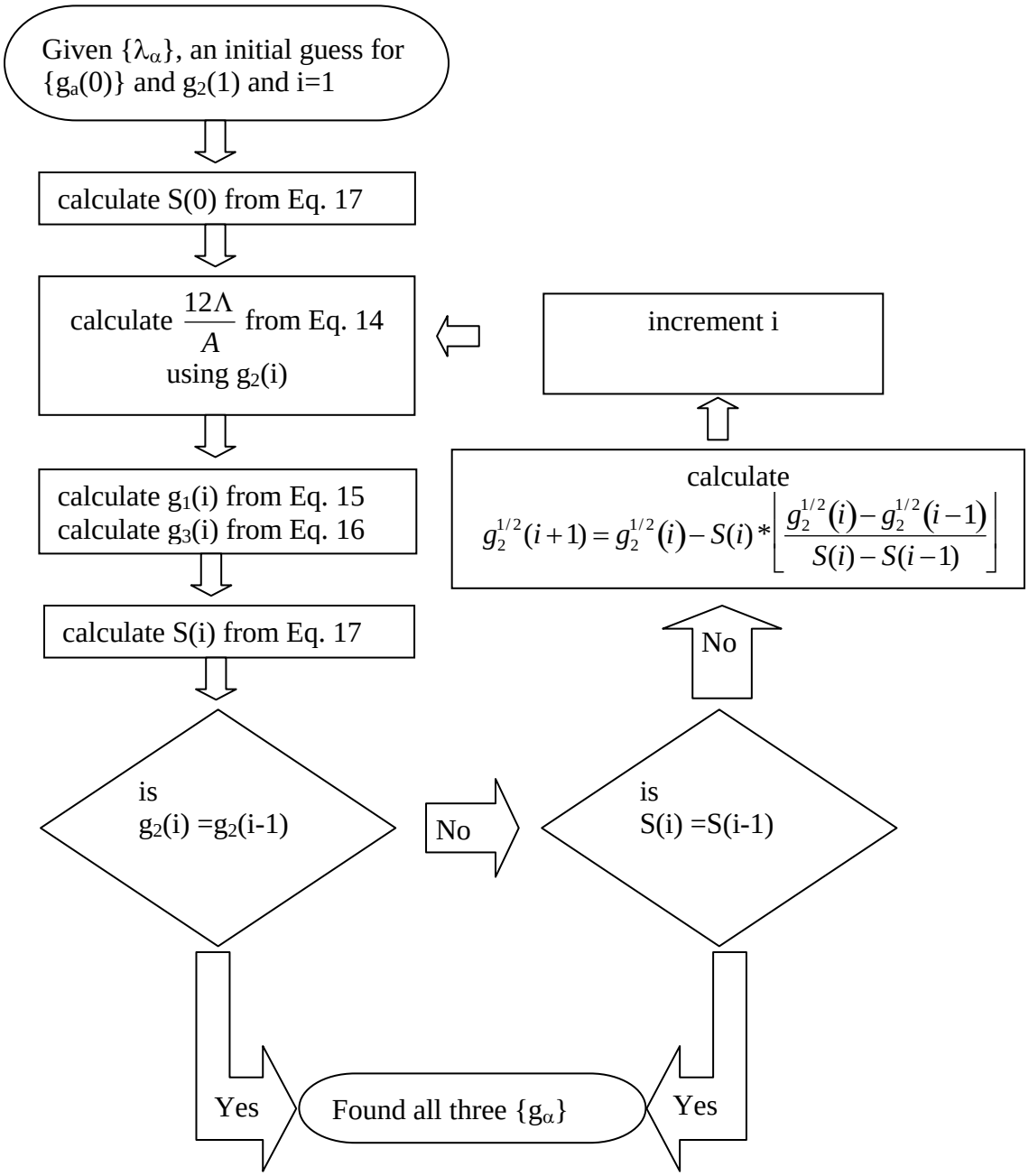

Figure 3.1: Flowchart of Procedure to Calculate Rubinstein-Panyukov Scaling Factors g_α

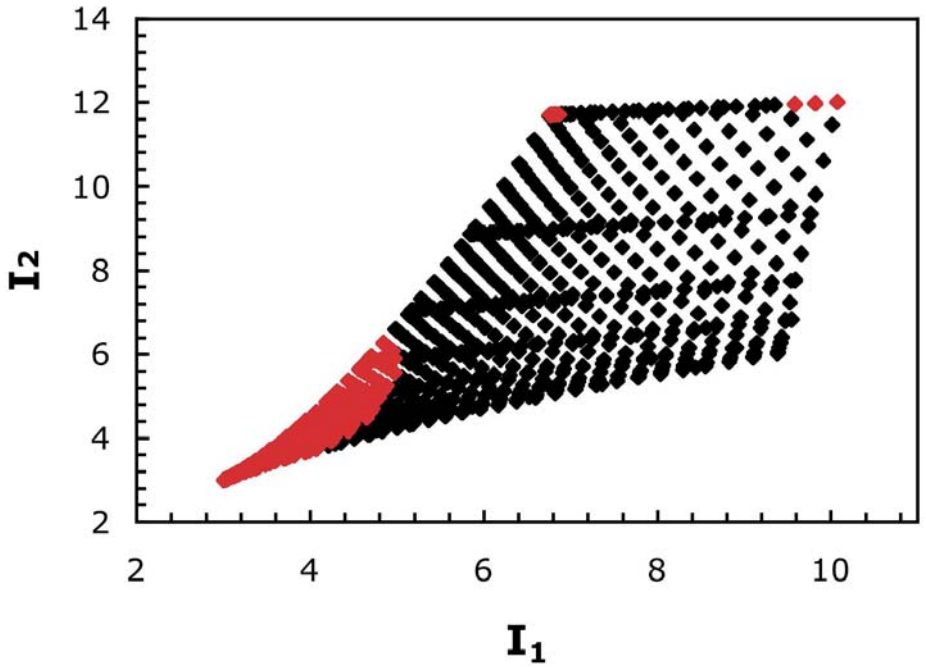

Figure 3.2: Deformation Space Used for Analytical Fit to Slip-Tube Model. The red points correspond to an error of greater than 1% when using a fit to the entire space. Black points correspond to an error of less than 1%.

When fitting to the strain energy determined by this map, the poorest fit was found for the small (I_1 and I_2 less than 6) deformations. This poorness of fit can be characterized as the difference between the fit strain energy and the calculated strain energy normalized by the calculated strain energy. In Figure 3.2, greater than 1% error is indicated in red. Thus, two fits (parameters shown in Table 3.1) were actually done for this data: one for $I_1 \le 5.0$ and $I_2 \le 6.27$ and one for the rest of the points.

Table 3.1. Analytical Strain Energy Fits to the Slip-Tube Model

Constant	$I_1 \le 5.0$ and $I_2 \le 6.27$	Outside the small I range
c10	0.0851661	0.0943634
c01	0.057562	0.043431
c11	-0.00334862	0.00113886
c20	-0.00478368	-0.00745304
c02	-0.00280587	-0.000935738
c21	-0.000418954	-0.000340933
c12	0.000503024	0.0000767233
c30	0.000841539	0.000553051
c03	0.000609627	-0.0000339206

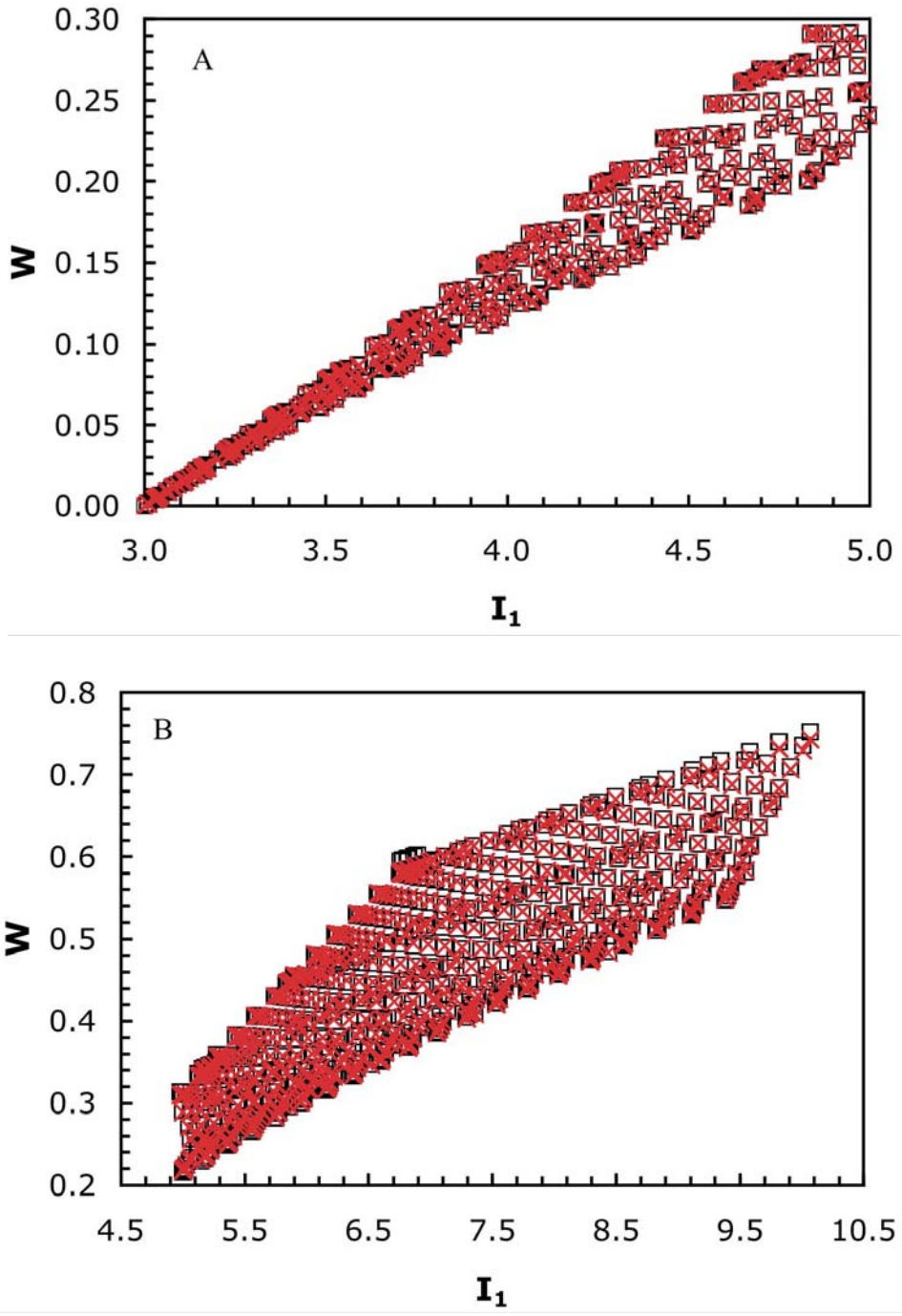

Figure 3.3: Strain Energies from the Slip-Tube Model. Comparison of Self-Consistent Calculation and Analytical Fit.

A) for $I_1 \leq 5.0$ and $I_2 \leq 6.27$. B) for the other deformations. Squares are the calculated strain energies from Eq. 22. The x's are from the fit to Eq. 18.

The benefit of doing two fits is shown in Figure 3.3. Small strain invariants correspond to small deformations. The errors in those fits are now considerably less than 1%. Indeed, most of the range has an error of less than 0.1%. The larger strain invariants have larger error. However, even the worst error seen is less than 2.5% with most of the errors less than 1%.

A point of concern is whether the artificiality of having two fits would cause anomalies in systems as they switch from one region to the other. Examining this region shows that anomalies are very small (deviation in the third significant figure) and that the deformation changes must be proceeding in small ($\Delta\lambda$=0.01) steps to see this anomaly. Representative plots are shown in Figure 3.4.

An interesting comparison is for a particular deformation mode. This can be done by self-consistently calculating $\{g_a\}$ from Eq. 12 to put in the strain energy formula (Eq. 22) and then calculating the strain energy from the analytical fit at the same stretch ratios. Uniaxial extension has a deformation according to

$$\lambda_1 = \lambda$$
$$\lambda_2 = \lambda_3 = \frac{1}{\sqrt{\lambda}} \quad (23)$$

Pure shear can be summarized as

$$\lambda_1 = \lambda$$
$$\lambda_2 = \frac{1}{\lambda}$$
$$\lambda_3 = 1 \quad (24)$$

The comparisons for these two deformation modes are shown in Figure 3.5 and Figure 3.6. Within the range of λ that was fit, the agreement is good (less than 1% relative error between using the full strain energy and fit strain energy). The agreement rapidly deteriorates for deformations outside the fit region.

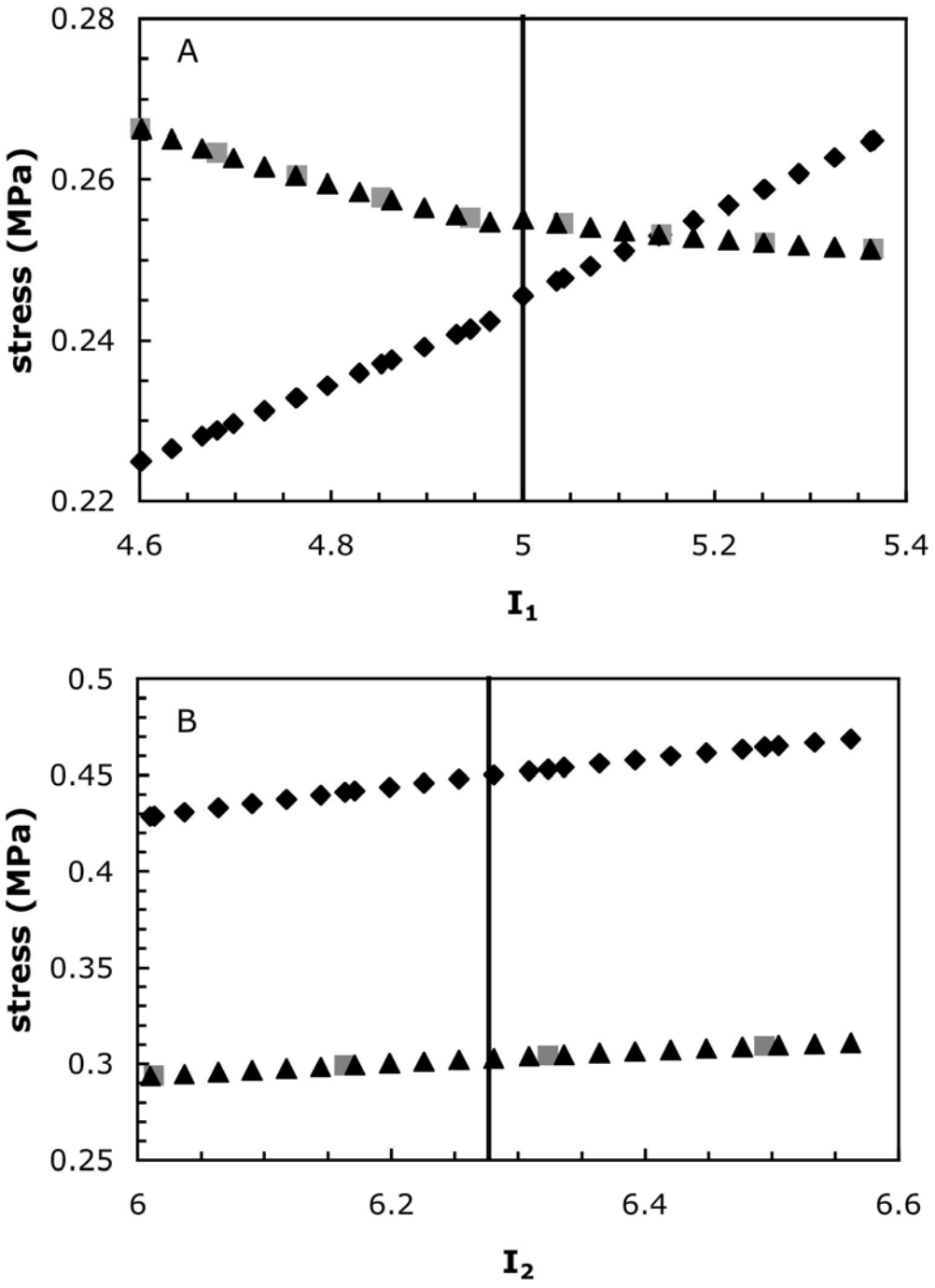

Figure 3.4: Examining Stress at the Crossover Point Between Analytical Fits to the Slip-Tube Model.

This is a system in uniaxial extension (x-direction) with G_c=0.177 MPa and G_3=0.177 MPa. A) Stress as a function of I_1. B) Stress as a function of I_2. Diamonds are stress in the x-direction, squares, in the y-direction, triangles, in the z-direction.

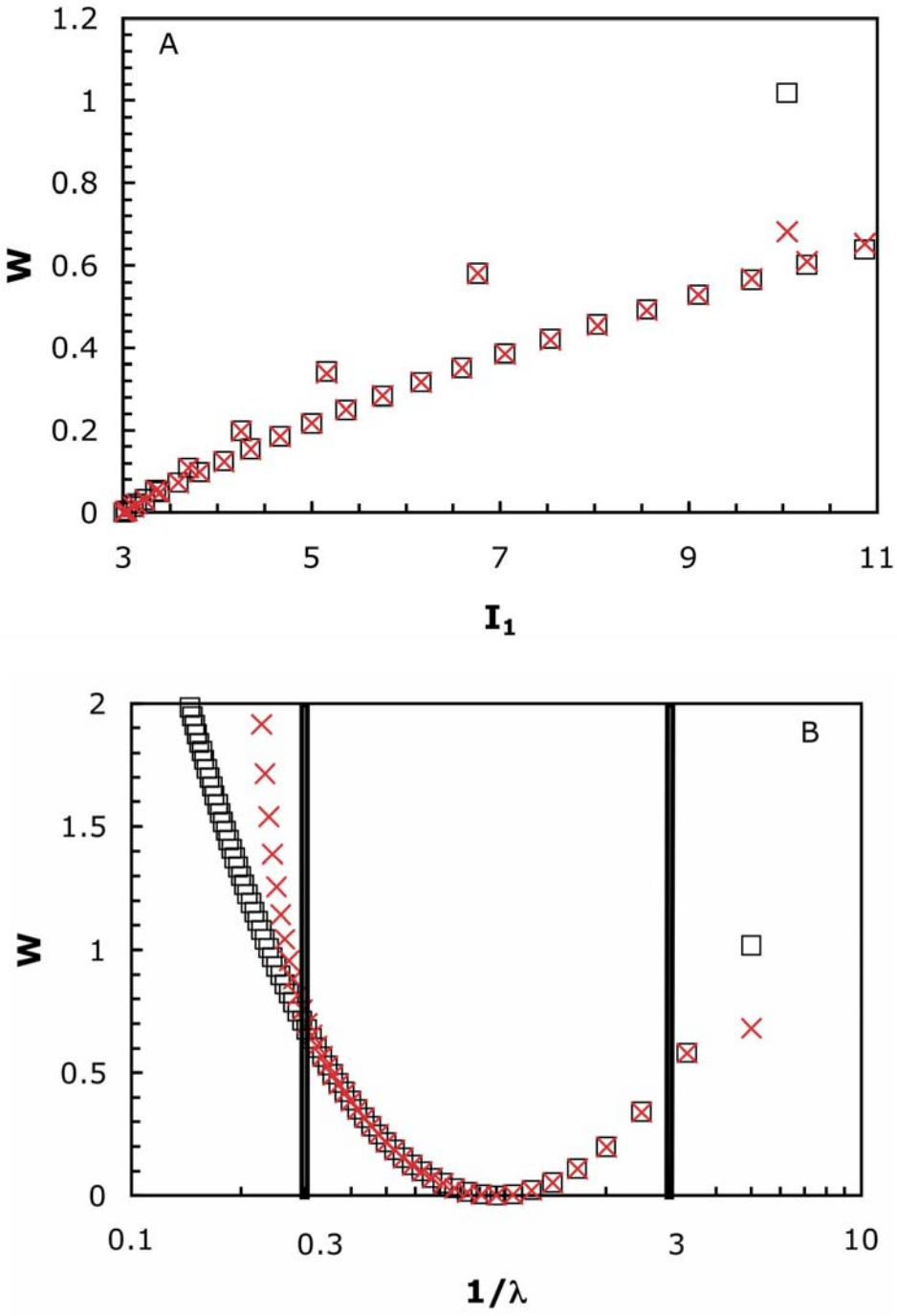

Figure 3.5: Strain Energies from the Slip-Tube Model. For Uniaxial Extension, Comparison of Analytical Fit and Self-Consistent Calculation.

A) plotted versus I_1 B) plotted versus $1/\lambda$. Squares are the calculated strain energies from Eq. 22. The x's are from the fit to Eq. 18.

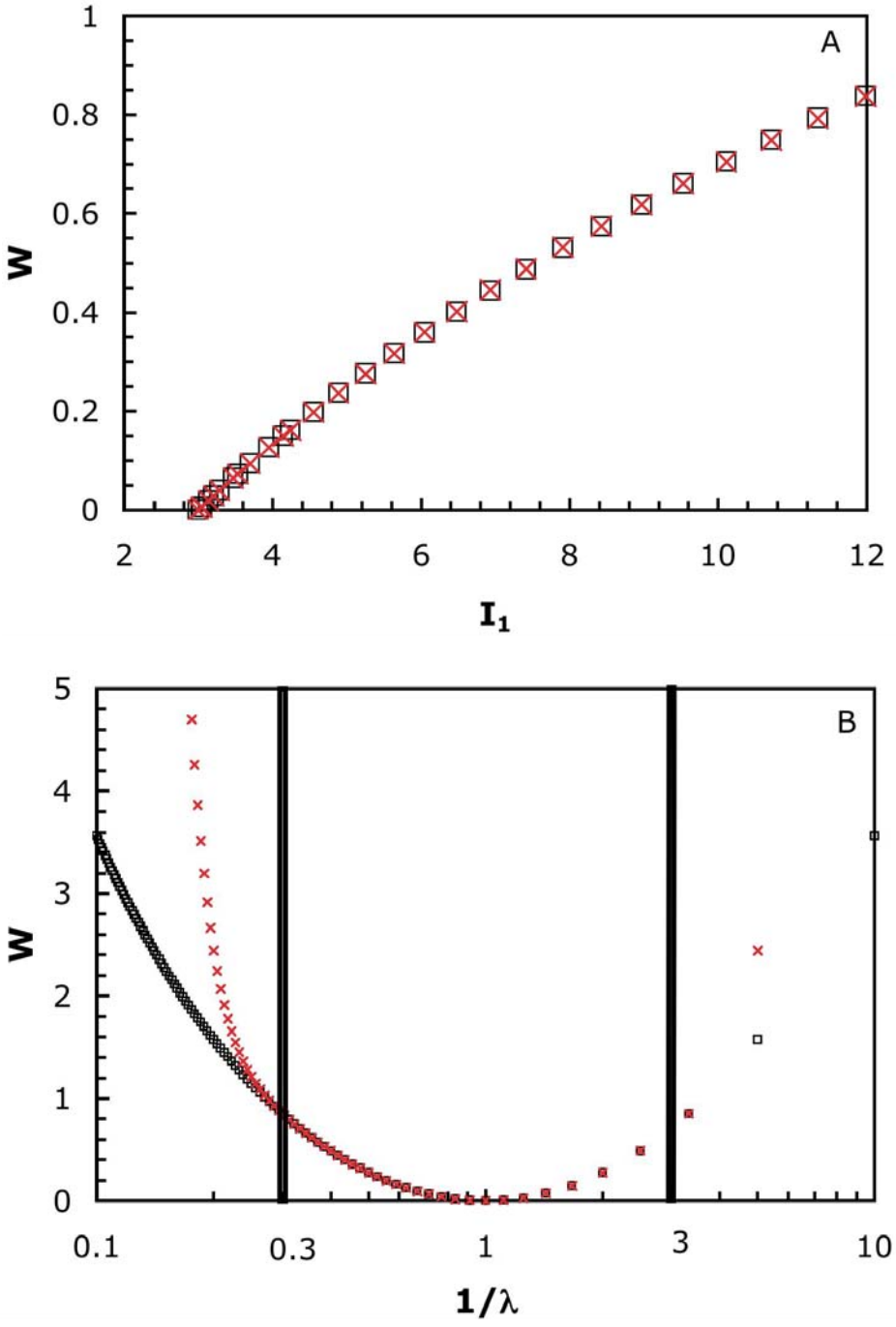

Figure 3.6: Strain Energies from the Slip-Tube Model. For Pure Shear, Comparison of Analytical Fit and Self-Consistent Calculation.

A) strain energy versus I_1. B) strain energy versus 1/λ. Symbols are same as in Figure 3.3.

3.2. Calculating Stress from Strain Energy

With the strain energy written in terms of principal stretches, the stress is determined from

$$\sigma_i = \lambda_i \frac{\partial W}{\lambda_i} + p$$

(25)

where p is a Lagrangian indeterminate multiplier depending on the specific deformation conditions. Using Eq. 18 to calculate the stress gives

$$\begin{aligned}\sigma_\alpha^{ST} &= 2\lambda_\alpha^2 c_{10} + 2\lambda_\alpha^2 c_{01} B + 2\lambda_\alpha^2 c_{11}\left[(I_2-3)+B(I_1-3)\right]+4\lambda_\alpha^2 c_{20}(I_1-3)\\ &+4\lambda_\alpha^2 c_{02}B(I_2-3)+2\lambda_\alpha^2 c_{21}\left[2(I_1-3)(I_2-3)+B(I_1-3)^2\right]\\ &+2\lambda_\alpha^2 c_{12}\left[(I_2-3)^2+2B(I_1-3)(I_2-3)\right]+6\lambda_\alpha^2 c_{30}(I_1-3)^2+6\lambda_\alpha^2 c_{03}B(I_2-3)^2\\ &+p\end{aligned}$$

(26)

where

$$B = \lambda_\beta^2 + \lambda_\gamma^2$$

(27).

To calculate the entire stress, the stress for the phantom model is added to the entanglement contribution

$$\sigma_\alpha^{Ph} = \lambda_\alpha^2 + p_2$$

(28)

where p_2 is another indeterminate Lagrangian multiplier. The general method to calculate the indeterminate multipliers is to subtract 1/3 the trace of the individual stress components and then add back a contribution from the bulk modulus. In uniaxial extension, one takes the difference of two stresses to eliminate the indeterminate multipliers.

The total stress can then be written as

$$\sigma_\alpha = 2G_e\sigma_\alpha^{ST} + G_c\sigma_\alpha^{Ph}$$

(29)

where

$$G_c = \nu k_B T \left(1 - \frac{2}{\phi}\right)$$

(30)

$$G_e = \frac{4}{7} A = \frac{4}{7} \frac{c k_B T}{N_e}$$

(31)

with ν as chain density, ϕ as crosslink functionality, k_B as Boltzmann's constant, T as temperature, c as the monomer density, and N_e as the entanglement spacing. The stress is written in Eq. 29 so that it matches with the results of Rubinstein and Panyukov.

Rubinstein and Panyukov[19] have an expression for the stress for uniaxial extension

$$\sigma_{\parallel} - \sigma_{\perp} = G_c\left(\lambda^2 - \frac{1}{\lambda}\right) + \frac{G_e}{0.74\lambda + \frac{0.61}{\sqrt{\lambda}} - 0.35}\left(\lambda^2 - \frac{1}{\lambda}\right) \tag{32}$$

where the stress is measured as the difference between the stresses parallel and perpendicular to the stretch direction and the stretch ratio is λ. Figure 3.7 shows this comparison. As seen with the strain energy, the error in the stress is much larger outside the fit range of deformation.

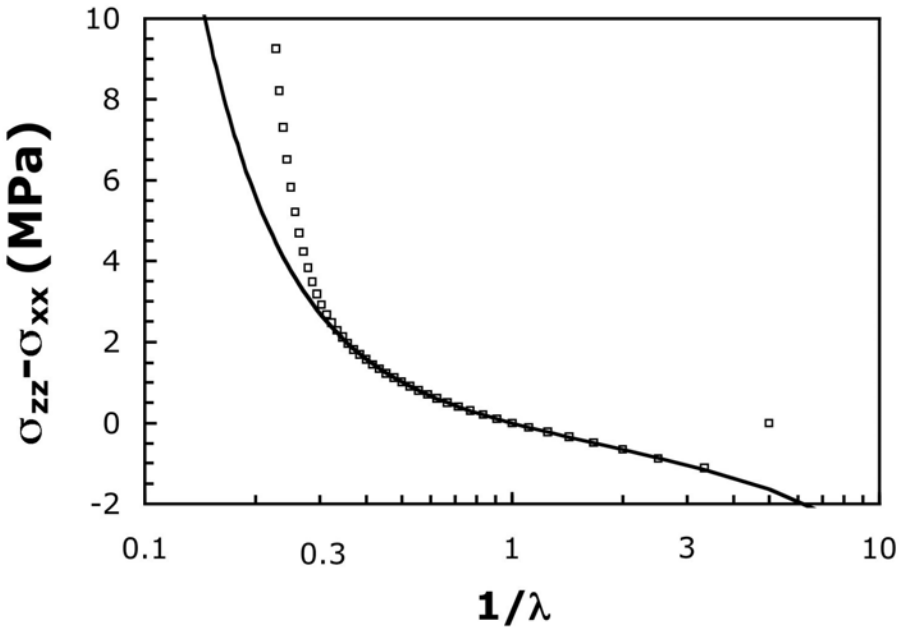

Figure 3.7: Uniaxial Stress from the Slip-Tube Model. Comparing Analytical Fit to Arbitrary Deformation with Analytical Fit to Uniaxial Extension.
Squares are calculated using Eq. 29 and the line is Eq. 32 with G_e=0.177 MPa and G_c=0.177 MPa.

4. COMPARISON OF FINITE ELEMENT CALCULATIONS WITH EXPERIMENT

To validate the model, comparison with experimental results is essential. Although the goal is to predict chemical aging over long times of decades, controlled experiments that provide enough information to use our model have not been performed[23]. However, accelerated aging experimental studies on butyl rubber and butyl o-rings are available in the literature.

As formulated from the simulations, the constitutive model is incompressible. This is a good approximation, but not appropriate for use with finite element. The material model as implemented in Adagio uses a nearly incompressible formulation and the augmented Lagrangian technique available in Adagio. This gives a more realistic response since rubber is nearly incompressible and the modulus will change as chemical aging occurs.

4.1. Physical Properties Required for Calculations

In addition to the reaction and strain histories, the finite element code requires elastic constants and the plateau modulus (if an entanglement contribution is desired) in order to perform calculations. While all of these quantities are measurable by experiment, no published studies have all of this information for the same sample. Therefore, we have made some approximations. Because our main objective is to match relative quantities (normalized stress relaxation and permanent set), the exact magnitude of the elastic constants will be unimportant as long as two conditions are met. First, the bulk modulus must be substantially larger than the shear modulus so that the Poisson's ratio is about 0.5. Second, the magnitudes must be large enough to prevent numerical problems with the finite element solvers. For example, stress is only accurate to about 0.01 units so working in the reduced space of one stress unit is unfeasible. Working in the physically reasonable range with stresses ranging from hundreds of psi to zero is acceptable.

Another difficulty is that crosslinking magnitudes are rarely reported in the literature for experimental aging studies. More commonly, normalized stress relaxation data are given. Crosslinking history can be inferred using normalized stress relaxation results by making a few assumptions and that procedure has been employed here on two experimental studies. The classic work on permanent set and the independent network hypothesis was done by Tobolsky and coworkers[6]. Consequently, their results on butyl rubber are used as one of the experimental data sets to validate the new model. The other experimental study used is work from researchers here at Sandia on butyl O-rings in compression. Both of these studies are accelerated aging (high temperature) experiments so that the reduction in stress can be observed in reasonable time.

The remainder of this section is the comparison of finite element calculations with results from stress relaxation experiments. Because only a single stress value is reported as a function of time, a uniform stress state can be assumed. This assumption allows for a simple cube of material to be used as the geometry. Calculations have been done with an o-ring geometry to observe stress distributions across the cross-section, but they are not suitable for validation purposes. For each experimental data set, the method of extracting the crosslinking history and the assumptions used are detailed. The resulting crosslink history is shown for each set and finite element results are given for continuous stress relaxation. Permanent set is predicted using that chemistry and is found to be in good agreement with the experimental data.

4.2. Tobolsky Experimental Data in Extension

Our particular interest here is the butyl gum data from Tobolsky's group (Figure 7 of Reference 6). Two stress relaxation experiments were performed on samples from the same cure batch. Consequently, the chemistry of both samples as a function of time is expected to be the same. Both procedures report the ratio of current stress with initial stress for the time of the test. The difference between the two types of investigation is their strain history. Continuous stress relaxation is the more common test. The sample is deformed and stress measurements are taken while the sample is held in the deformed state. This approach provides information about the effective stage one network as a function of time. In this case, the sample was uniaxially deformed to a stretch ratio of λ_2=1.5. The intermittent stress relaxation procedure periodically stretches the sample to λ_2 for long enough to take a stress reading and then releases the sample. As a result, the chemical reactions take place primarily in the unstretched state. The intermittent method provides information about the total crosslinking density of the sample. The data for butyl gum at 130 ^{0}C is shown in Figure 4.1.

Some type of kinetics must be assumed to get G_1 and G_2 (moduli of stage 1 and stage 2 networks). Scission of stage 1 is likely to be first order and for times less than 1.35 hours, crosslink density stays constant so scission and crosslinking occur at equal rates. Under those conditions,

$$\frac{G_1^{eff}}{G_1^*} = \frac{1}{2-\exp(-kt)}; \qquad G_1 = G_1^* \exp(-kt); \qquad G_2 = G_1^* \left(1-\exp(-kt)\right) \tag{33}$$

G_1* can be identified as the shear modulus. Fitting the continuous stress relaxation data (which can be identified with G_1^{eff}/G_1*) yields k=1.54 h^{-1}. We assume that the first network continues to scission with first order kinetics; however, the second network no longer crosslinks at the same rate. We calculate G_2 after aging time = 1.35 hours using the continuous stress relaxation from the definitions of G_1^{eff} and Φ and solving for G_2. The resulting expression is

$$\frac{G_2}{G_1^*} = \frac{\left[\frac{G_1^{eff}}{G_1^*} - \exp(-kt)\right]\left(1 + \frac{G_2^*}{G_1^*}\right)}{1 - \exp(-kt)} \quad (34)$$

G_2* is the maximum in G_2 up to the current time and is found through enforcing self-consistency. We ensure that the values of G_2 obtained from first-order kinetics and Eq. 34 match at time = 1.35h with the difference between the two cases added as an offset to all later G_2.

Another complication occurs as the original network scissions below its gel point. New crosslinks formed after this point will not contribute to stress transfer. Chemically, no difference exists between a first and second stage crosslink. Thus, second stage crosslinks also undergo scission, but they may reform. Memory of the original network fades as fewer crosslinks were formed under its influence. Thus, accounting for crosslinks formed at λ_2 after the original network has decayed below its gel point is necessary. The intermittent stress relaxation is the sum of all crosslink contributions. The magnitude of these new crosslinks can be determined by difference

$$\frac{G_2^{\beta}}{G_1^*} = \frac{F^{\text{int}}}{F_0} - \frac{G_1}{G_1^*} - \frac{G_2^{\alpha}}{G_1^*} \tag{35}$$

where $G_2{}^{\alpha}$ is stage two crosslinks formed while the original network existed and $G_2{}^{\beta}$ denotes stage two crosslinks formed after the original network disintegrated. Eq. 34 is actually only for $G_2{}^{\alpha}$. These three contributions are shown in Figure 4.2 based on the initial shear modulus having a value of 109 psi. For the finite element calculations, a bulk modulus of 34.0×10^3 psi was used. This gives a Poisson's ratio of 0.498. Combining the chemistry and the elastic constants in the finite element calculation produces the continuous stress relaxation shown as black curve in Figure 4.1. This is in excellent agreement with the experiment, as one would expect since, in essence, this data was fit. This procedure verifies that the computer code for the model was correctly implemented.

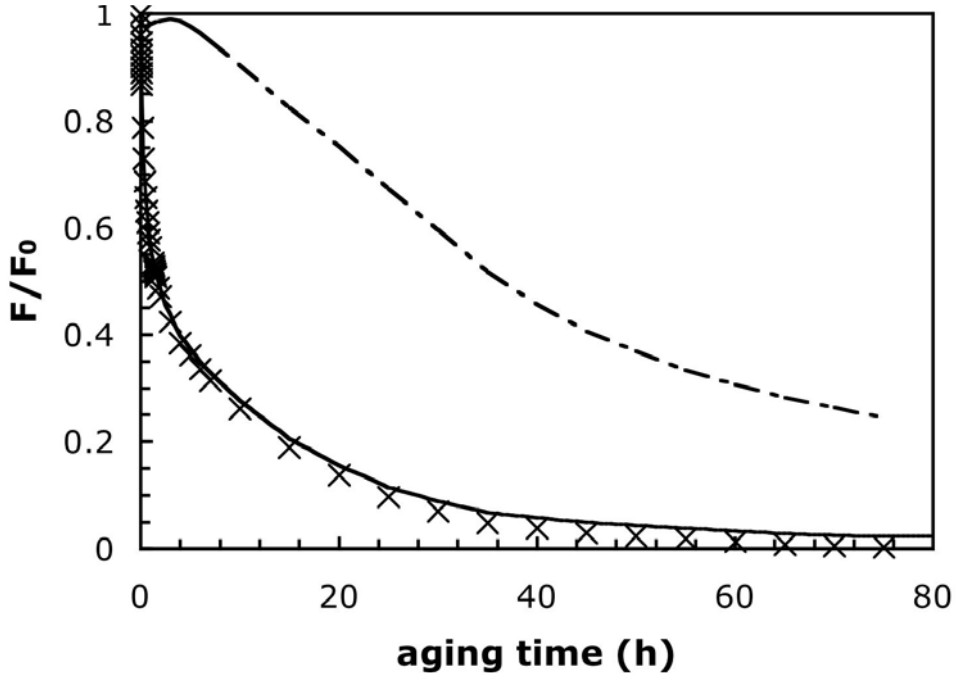

Figure 4.1: Stress Relaxation of Butyl Gum. Comparison of Experimental Data from the Tobolsky Group[6] and Finite Element Calculations.

The sample is butyl gum in uniaxial extension (λ_2=1.5) at 130 ^{0}C. The dashed line is intermittent stress relaxation data; the x's are continuous relaxation data. The solid line is finite element results using the fit parameters as described in the text.

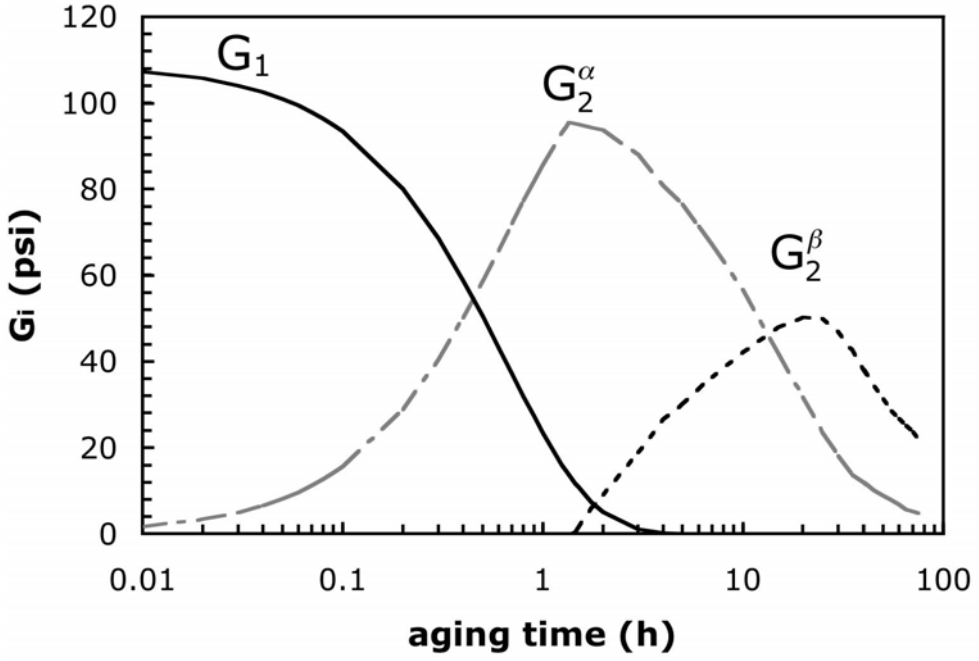

Figure 4.2: Crosslinking History Deduced from the Tobolsky Data[6]

A more stringent test is to predict permanent set. The finite element calculation was performed for the continuous stress relaxation test with restart files written at regular intervals. The finite element calculation for permanent set begins with one of the restart files. With the chemistry fixed for the network at that time, the sample was deformed back to the original shape. The stress was tracked during the deformation and the stretch ratio corresponding to the zero stress deformation was noted as λ_s. The permanent set can then be calculated from

$$PS = \frac{\lambda_s - 1}{\lambda_2 - 1} * 100 \quad (36)$$

Figure 4.3 compares the finite element results with the experimental data. The agreement between our predictions and experiment is quantitative.

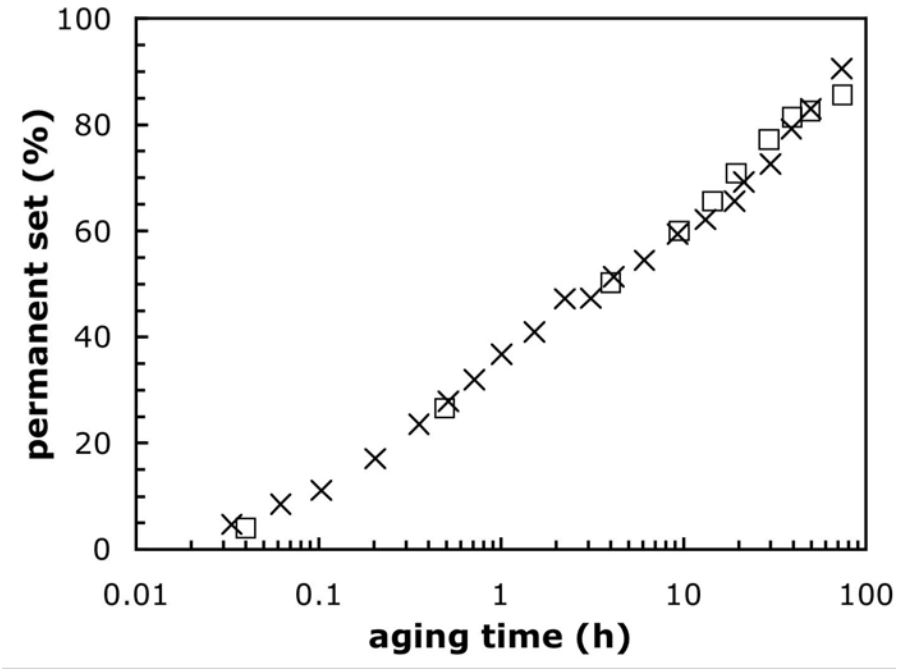

Figure 4.3: Permanent Set Comparison for Finite Element Calculation and Tobolsky Data[6]

Experimental data are denoted by x's and finite element calculations are squares.

4.3. Sandia Experimental Data in Compression

Gillen, Celina, and Bernstein[24] have reported sealing force relaxation data for o-rings from Burke Rubber Company (Compound 4061) at 125 ^{0}C. The data used was extracted from Figure 8 of Reference 24. Times reported here are aging times to coincide with those reported in Reference 24. The nominal deformation corresponds to λ_2=0.75.

Unfortunately, only continuous stress relaxation data were reported so less information is available directly from experiment.

A shear modulus of 146 psi and a bulk modulus of 34.0×10^3 psi were used. To fully explore the model, the entanglement contribution was estimated from literature data. Graessley[25] reports a plateau modulus of 32×10^4 Pa for polyisobutylene at 140 ^{0}C. Converting this for use in the slip-tube model at 125 ^{0}C involves a temperature conversion, a unit conversion, and multiplying by 4/7

$$G_e = \frac{4}{7} G_N^0 \frac{T_{desired}}{T_{original}}$$

$$G_e = \frac{4}{7} \left[32 * 10^4 \text{Pa}\right] \frac{398\text{K}}{413\text{K}} \left[\frac{14.7\text{psi}}{101325\text{Pa}}\right] = 26\text{psi}$$

(37)

This means that G_1^*=120 psi (subtracting G_e from the shear modulus). Including the entanglement contribution slightly complicates the calculation of the crosslinking history from the stress relaxation. The continuous stress relaxation is

$$\frac{F^{cont}}{F_0} = \frac{G_1^{eff} + f(\lambda) G_e}{G_1^* + f(\lambda) G_e} = \frac{\frac{G_1^{eff}}{G_1^*} + \frac{f(\lambda) G_e}{G_1^*}}{1 + \frac{f(\lambda) G_e}{G_1^*}}$$

(38)

where f(0.75)=1.10 as determined from the uniaxial slip-tube function[19]. Letting

$$F_e = \frac{f(\lambda) G_e}{G_1^*} = 0.23$$

(39)

eq. 38 can be written explicitly for G_1^{eff} as

$$\frac{G_1^{eff}}{G_1^*} = \frac{F^{cont}}{F_0} + \left[\frac{F^{cont}}{F_0} - 1\right] F_e$$

(40)

Using this relation, the effective stage one crosslinks were determined and the first order kinetics with equal rates crosslinking and scission applied (Eq. 33). This gives a rate constant k=0.067 h^{-1} up to a time of 5.86 h. G_2^*/G_1^*=0.38 from applying Eq. 34 during calculation of the G_2^{α}. The G_2^{β} were determined assuming that equal rates crosslinking and scission still hold after the time of 5.86 h. This will overestimate G_2^{β} since no provision is made for scission, even if the rate assumption is correct. The crosslink history determined for this sample is shown in Figure 4.4 and the comparison with experiment is shown in Figure 4.5. As before, the agreement between calculated stress relaxation and

experiment is good, further verifying the proper implementation of the model in the computer code.

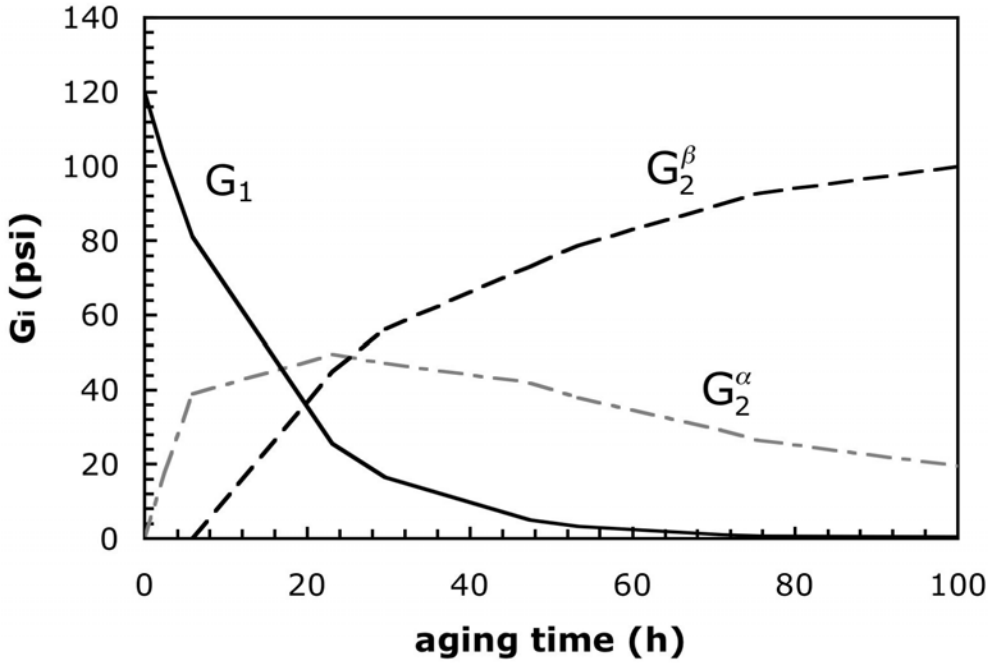

Figure 4.4: Crosslinking History for Butyl O-ring

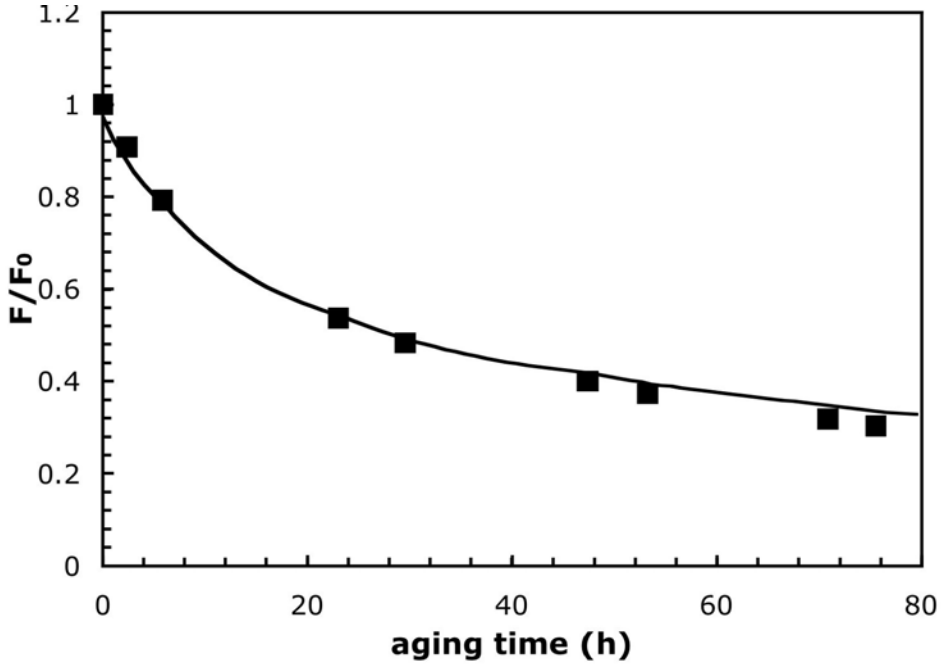

Figure 4.5: Continuous Stress Relaxation. Comparison of Finite Element Calculations with Experimental Results from Gillen, Celina, Bernstein[24]

Data is for o-ring from Burke Rubber Company (Compound 4061) at 125 ^{0}C. Symbols are experiment; line is finite element calculation.

Permanent set predictions were made using this crosslinking history in the finite element code. As can be seen in Figure 4.6, the finite element predictions agree well with the experiment. Because of the assumption of equal rates of crosslinking and scission, the permanent set is likely to be too large at long time which corresponds to small stress and higher permanent set. This is observed in Figure 4.6 where the two small permanent set points are closer to the experimental line than the two large permanent set points.

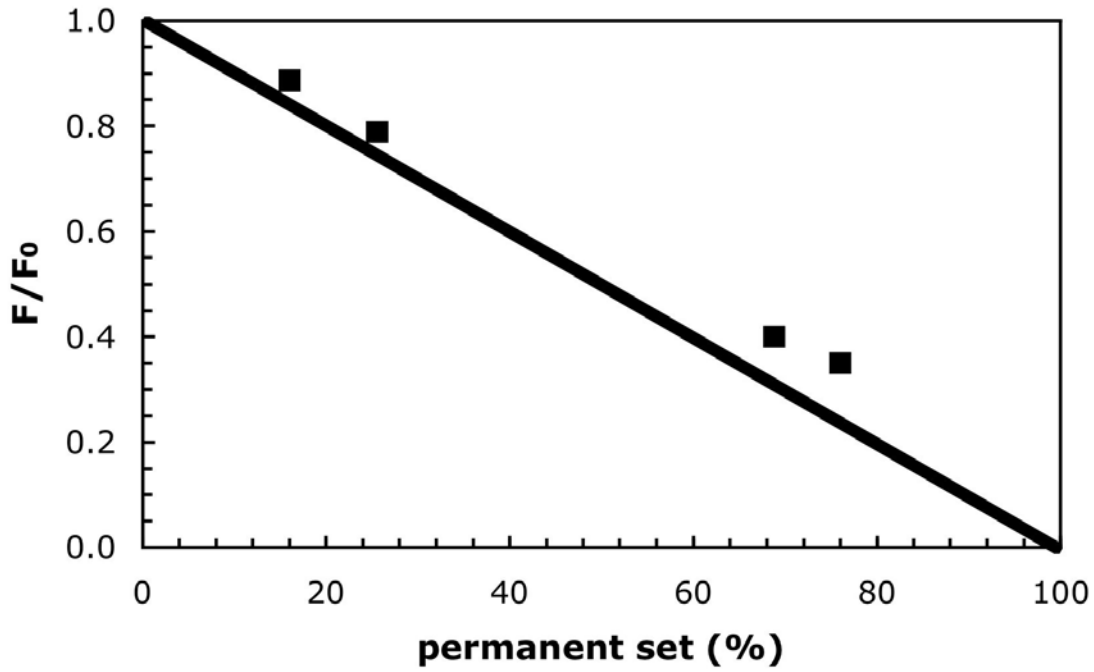

Figure 4.6: Permanent Set for Butyl Rubber in Compression
Symbols are from finite element calculation; line is derived from experiment as given in Gillen, Bernstein, and Wilson[4].

5. CONCLUSIONS

Using molecular dynamics simulations, we have developed a constitutive model for the crosslinking and scission of rubber networks in deformed states. This constitutive model is based on some well-established models from the literature and a few often-neglected points. The independent network hypothesis proposed by Tobolsky[6] in the 1940's is used in conjunction with the slip-tube model[19] of Rubinstein and Panyukov. This allows for the effects on the resulting network arising from both chemical crosslinks and physical entanglements to be included. The independent network hypothesis has been demonstrated to be valid for crosslinking in deformed states through simulation. Classical rubber elasticity models only require the relative crosslinking density of the two networks. However, permanent set determined from simulations showed that the crosslinking density of the original network also is a factor. The entanglements trapped by the original network must be included in the stress calculation and the slip-tube model ably captures this phenomenon.

To include the effects of scission of the original network, the independent network hypothesis has been modified to use effective crosslink densities. If scission of the original network occurs after crosslinking of a second network, a memory effect is seen. Some fraction of that second network will adopt the role of the original network, effectively acting as stage one crosslinks. This fraction can be quantified through stress transfer functions. The stress transfer function proposed by Fricker (based on theoretical considerations of phantom networks[20]) was found to agree with a model-free determination of the stress transfer functions from simulation.

This constitutive model has been implemented into the finite element code Adagio. In order to do this, the slip-tube model was modified to be computationally tractable. An analytical fit was applied to strain energies calculated from the original self-consistent formulation. This fit was seen to match the self-consistent formulation over the expected deformation range for an o-ring and a uniaxial extension in an experimental system. The model developed from simulation was incompressible. The model implemented in Adagio is nearly incompressible, taking advantage of the augmented Lagrangian technique available in the finite element code.

The model was validated through comparison with accelerated aging experiments on butyl rubber. Experimental data in uniaxial extension and an o-ring in compression were chosen as the test cases. Crosslinking history was deduced from stress relaxation measurements and used in conjunction with estimates of elastic constants to perform finite element calculations. Continuous stress relaxation results from those calculations were in good agreement with the experimental data. The deduced chemistry was then used in finite element calculations to predict permanent set. Those permanent set predictions are also in excellent agreement with the experimental data.

6. FUTURE WORK

The Kansas City plant has been working on new butyl rubber formulations specifically tailored for Sandia. This provides an opportunity to plan complementary simulations and experiments to investigate this new formulation. In this way, all the experimental data necessary to validate the model can be obtained. In addition, simulations using recently developed reactive forcefields can be used to help elucidate the chemical reaction mechanisms.

Simulations are planned to validate the reactive forcefields using experimental data for chemical aging of polypropylene[26]. This polypropylene system was a pure system and was specially synthesized to scrutinize reactive species. After the forcefields have been validated for chemical aging in olefins, they may be suitable for studying the chemical aging of the more complicated butyl systems. As an efficiency measure, the simulations to validate the forcefields can be run while the experiments on the new butyl formulations are being performed. In that way, when the experimental butyl data becomes available, the constitutive model can be tested and the new simulations on the butyl may be ready to begin.

Another possible avenue of exploration is the effect of filler. While most o-rings have filler added to enhance the mechanical properties, the microscopic interactions between the filler particles and the polymer matrix are not well understood. Micromechanics calculations could help investigate those interactions.

Refinements to the stress transfer functions are also possible. The current equations were developed from sequential crosslinking and scission. Simultaneous crosslinking and scission may need a slightly different form. We have developed a logical extension of the Fricker formula for two stages to multiple stages, with only cursory testing. More comprehensive testing would be wise.

7. REFERENCES

1. J. G. Curro and E. A. Salazar "Physical and Chemical Stress Relaxation of Elastomers" J. Appl. Polym. Sci. **19**, 2571 (1975).
2. E. A. Salazar, J. G. Curro, and K. T. Gillen "Physical and Chemical Stress Relaxation of a Fluoroelastomer" J. Appl. Polym. Sci. **21**, 1597 (1977).
3. J. G. Curro and E. A. Salazar "Mechanical Behavior of O-Rings" Rubber Chem. Technol. 46, 530 (1973).
4. K. T. Gillen, R. Bernstein, and M. H. Wilson "Predicting and Confirming the Lifetime of O-rings" Polym. Degrad. Stabil. **87**, 257 (2005).
5. J. Budzien, D. C. S. Lo, J. G. Curro, A. P. Thompson, G. S. Grest, and D. Rottach "Constitutive Models for Rubber Networks Undergoing Simultaneous Crosslinking and Scission" SAND2005-7357.
6. R. D. Andrews, A. V. Tobolsky, and E. E. Hanson, "The Theory of Permanent Set at Elevated Temperatures in Natural and Synthetic Rubber Vulcanizates" J. Appl. Phys. **17**, 352 (1946).
7. D. R. Rottach, J. G. Curro, G. S. Grest, and A. P. Thompson, "Effect of Strain History on Stress and Permanent Set in Crosslinking Networks: A Molecular Dynamics Study" Macromolecules **37**, 5468 (2004).
8. L. R. G. Treloar *The Physics of Rubber Elasticity* 2nd ed. Oxford University Press, London (1958) p.155.
9. E. Guth and H. M. James "Elastic and thermoelastic properties of rubberlike materials: A statistical theory" Ind. Eng. Chem. **33**, 624 (1941).
10. H. M. James and E. Guth "Theory of rubber elasticity for development of synthetic rubbers" Ind. Eng. Chem. **34**, 1365 (1942).
11. M. Mooney "A Theory of Large Elastic Deformation" J. Appl. Phys. **11**, 582 (1940).
12. R. S. Rivlin "Large Elastic Deformations of Isotropic Materials. IV. Further Developments of the General Theory" Phil. Trans. Roy. Soc. (London) A **241**, 379 (1948).
13. R. W. Ogden *Non-linear Elastic Deformations* Dover Publications, Mineola, NY (1997) p. 221.
14. G. S. Grest and K. Kremer "Statistical Properties of Random Cross-Linked Rubbers" Macromolecules **23**, 4994 (1990).
15. S. Plimpton "Fast Parallel Algorithm for Short-Range Molecular Dynamics" J. Comp. Phys. **117**, 1 (1995). http://www.cs.sandia.gov/~sjplimp/lammps.html
16. A. P. Thompson "Molecular Simulation of Reacting Systems" SAND2002-0604.
17. D. R. Rottach, J. G. Curro, J. Budzien, G. S. Grest, C. Svaneborg, and R. Everaers "Permanent Set of Cross-Linking Networks: Comparison of Theory with Molecular Dynamics Simulations" Macromolecules **39**, 5521 (2006).
18. B. Erman and P. J. Flory "Theory of elasticity of polymer networks. II. The effect of geometric constraints on junctions" J. Chem. Phys. **68**, 5363 (1978).
19. M. Rubinstein and S. Panyukov "Elasticity of Polymer Networks" *Macromolecules* **35**, 6670 (2002).
20. H. S. Fricker "The Effects on Rubber Elasticity of the Addition and Scission of Cross-links under Strain" Proc. Roy. Soc. London Ser. A Math Phys Sci **335**, 267 (1973).

21. W. H. Press, S. A. Teukolsky, W. T. Vetterling, B. P. Flannery *Numerical Recipes in Fortran 77* 2nd ed. Cambridge University Press NY (1992) p.179 has the analytical solution to a cubic equation.
22. E. Kreyszig *Advanced Engineering Mathematics* 8th ed. John Wiley & Sons, NY (1999) p.846.
23. A long-term aging study has been published, but the resulting data is unsuitable for the purposes of validation. R. P. Brown and T. Butler "Natural Ageing of Rubber: Changes in Physical Properties over 40 Years" Rapra Technology Limited, Shawbury, Shropshire, UK (2000).
24. K. T. Gillen, M. Celina, and R. Bernstein "Validation of improved methods for predicting long-term elastomeric seal lifetimes from compression stress-relaxation and oxygen consumption techniques" Polym. Degrad. Stabil. **82**, 25 (2003).
25. W. W. Graessley *Polymeric Liquids and Networks: Structure and Properties* Garland Science, NY (2004) p. 454.
26. D. M. Mowery, R. A. Assink, D. K. Derzon, S. B. Klamo, R. L. Clough, and R. Bernstein "Solid-state ^{13}C NMR investigation of the oxidative degradation of selectively labeled polypropylene by thermal aging and gamma-radiation" Macromolecules 38, 5035 (2005).

APPENDIX A: SUMMARY OF MATERIAL MODEL

A.1. Introduction

This material model was developed for the crosslinking and scission of rubbers in multiple strained states. The basis of the model is a modification of the independent network hypothesis[i]. In the independent network hypothesis, networks have a state of ease (i.e., zero stress) at the deformation state in which they were formed. Thus, crosslinking in a strained state will lead to additional networks being formed. The resulting stress on the entire sample is the sum of the individual stresses from each network. This model as implemented in Strumento is capable of having five different networks with corresponding states of ease.

Scission requires a modification to the independent network hypothesis. Because of the coupling between the strain history and the reaction history, the networks that form in the strained states have a dependence upon the prior topology of the sample. This can be seen schematically in Figure A.1. The system is crosslinked once in an isotropic state. After deformation, the system is crosslinked for a second time in the deformed state. These crosslinks are not necessarily chemically different from the first crosslinks, but their state of ease will be the deformed state. If the first network undergoes scission, the stress will decrease. However, the stress will not decrease as far as the independent network predicts. Some of the second stage crosslinks will continue to hold the sample in the same deformation and effectively act as first stage crosslinks. From Figure A.1, this result is not a one-for-one exchange, but is instead a consequence of several crosslinks acting together. In this manner, the sample retains memory of the coupling of the deformation and reaction histories The term stress transfer is used to denote the result of crosslinks from a particular network acting as crosslinks from a different network. The stress transfer functions (as defined under the section titled "Parameter Explanations") quantitatively describe the portion of a given network acting as a different network.

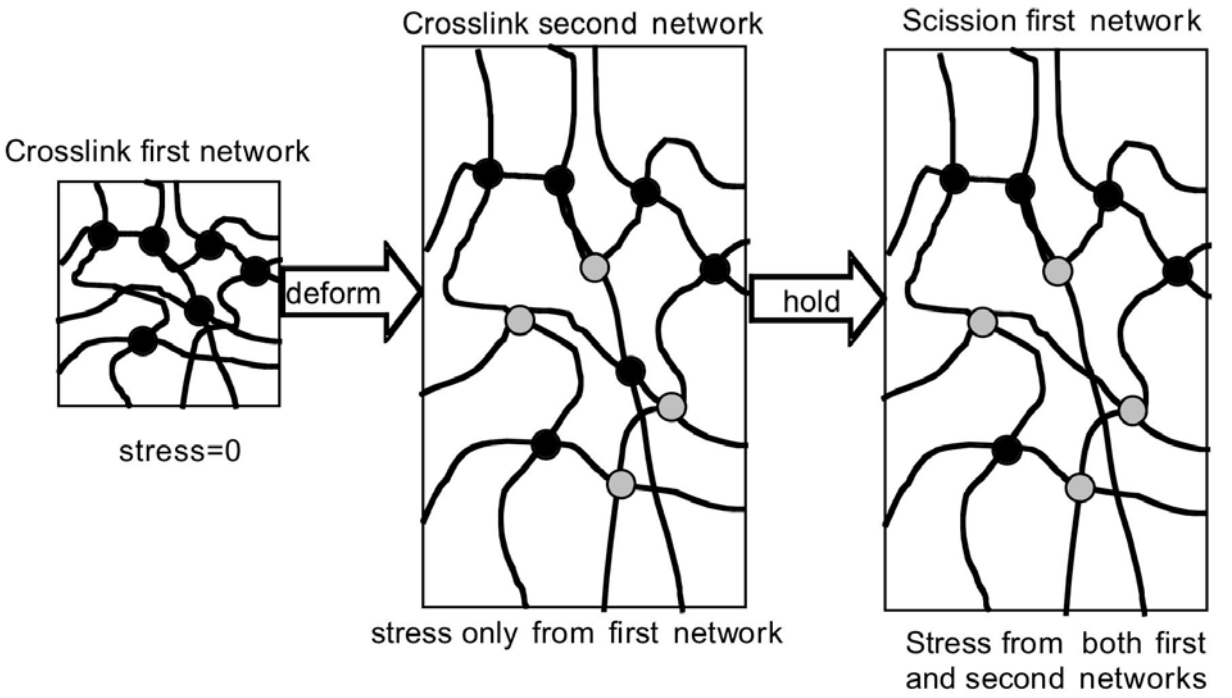

Figure A.1: Schematic of a Two-Stage Network Undergoing Crosslinking and Scission.

A.2. Strain Energy Formulations

As implemented, this material model actually has three strain energy types available. This feature allows for comparison of the effects of chemical crosslinks, physical entanglements, and stress transfer on the sample stress. This section gives the formulae for calculation of the stresses from the three strain energy types. The section labeled "Parameter Explanations" details how to calculate the values that are required for the input deck.

A.2.1. Strain Energy Type 1: Affine Model

This strain energy only includes the effects of chemical crosslinks. The affine model of rubber elasticity is used. For a given stage i, the stress is calculated as

$$\underline{\underline{\sigma}}_i^{affine} = \frac{G_i}{\det\left(\underline{\underline{\lambda}}\right)} \underline{\underline{\lambda}}\,\underline{\underline{\lambda}}_i^{-1} \left[\underline{\underline{\lambda}}_i^{-1}\right]^T \underline{\underline{\lambda}}^T + p \tag{A.1}$$

where G_i is the modulus of stage i (number of chains formed during stage i per original volume multiplied by RT), $\underline{\underline{\lambda}}$ is the deformation gradient tensor relative to the original state, and $\underline{\underline{\lambda}}_i$ is the deformation gradient at which the i stage crosslinks were inserted. p is an indeterminate Lagrangian multiplier.

The total Cauchy stress is calculated from

$$\underline{\underline{\sigma}} = \sum_{i=1}^{nstages} \underline{\underline{\sigma}}_i^{affine} - \underline{\underline{I}} \frac{Tr\left(\underline{\underline{\sigma}}_i^{affine}\right)}{3} + \frac{G_i}{G}\kappa \ln\left[\frac{\det\left(\underline{\underline{\lambda}}\right)}{\det\left(\underline{\underline{\lambda}}_i\right)}\right]$$

(A.2)

where κ is the bulk compressibility of the entire sample and G is the sum of moduli for stages not in their state of ease.

A.2.2. Strain Energy Type 2: Affine Model with Ogden Entanglements

This strain energy has chemical crosslinks using the affine model and an entanglement contribution using the Ogden model[ii]. Stress for the Ogden model can be written in terms of principal stretches as:

$$\sigma_k^{ogden} = \frac{G_{e,1}}{\det\left(\underline{\underline{\lambda}}\right)}\lambda_k^{a1} + \frac{G_{e,2}}{\det\left(\underline{\underline{\lambda}}\right)}\lambda_k^{a2} + p$$

(A.3)

where $G_{e,1}$ and $G_{e,2}$ are moduli (effectively, number of entanglements per original volume multiplied by RT), a_1 and a_2 are chosen constants, and λ_k is a principal stretch. p is again an indeterminate Lagrangian multiplier. The total Cauchy stress is then calculated as

$$\underline{\underline{\sigma}} = \underline{\underline{\sigma}}^{ogden} - \underline{\underline{I}} \frac{Tr\left(\underline{\underline{\sigma}}^{ogden}\right)}{3} + \frac{G_{e,1}}{G}\kappa \ln\left[\det\left(\underline{\underline{\lambda}}\right)\right] + \sum_{i=1}^{nstages}\left\{\underline{\underline{\sigma}}_i^{affine} - \underline{\underline{I}} \frac{Tr\left(\underline{\underline{\sigma}}_i^{affine}\right)}{3} + \frac{G_i}{G}\kappa \ln\left[\frac{\det\left(\underline{\underline{\lambda}}\right)}{\det\left(\underline{\underline{\lambda}}_i\right)}\right]\right\}$$

(A.4)

where G now includes $G_{e,1}$ as part of the sum of moduli not in their state of ease. $G_{e,2}$ is not included as part of the G sum. Note that both entanglement terms are assumed to have the original deformation as their state of ease. Physically, this corresponds to the fact that the initial gelation traps the maximum number of entanglements so that additional crosslinks do not trap any additional entanglements. This may not be true for lightly crosslinked networks (see Ref. iii); however, rubbers used in standard applications are well above their gel points.

The Mooney-Rivlin form is a special case of the Ogden model with a_1=2.0 and a_2=-2.0. While the Ogden model can be used by itself to calculate crosslinked networks without entanglements, the current implementation will only support one such network with its state of ease at the original deformation.

A.2.3. Strain Energy Type 3: Phantom Model with Slip-tube Entanglements

This strain energy has chemical crosslinks using a phantom model and an entanglement contribution from the slip-tube model[iv]. The form of the phantom stress is the same as Eq. A.1; however, the phantom model has a modulus that is half that of the affine model (for tetrafunctional crosslinks). The slip-tube model has been fit to a power series in the first two strain invariants for a series of deformations.

$$W = \sum_{j=0}^{\infty}\sum_{k=0}^{\infty} c_{jk}\left(I_1 - 3\right)^j \left(I_2 - 3\right)^k$$
(A.5)

where c_{jk} are fit parameters and the strain invariants are defined as

$$I_1 = \lambda_1^2 + \lambda_2^2 + \lambda_3^2$$
(A.6)
$$I_2 = \lambda_1^2\lambda_2^2 + \lambda_2^2\lambda_3^2 + \lambda_3^2\lambda_1^2$$
(A.7)

in terms of principal stretches (λ_i). The deformations were chosen so that all three stretches lie in the range of 0.3 to 3.0 and the set of stretches is consistent with incompressibility. A warning will print if the given deformation is outside this fit range. In fact, the region was fit in two segments: one for small strain invariant and one for larger strain invariant. For deformations in which one invariant is large and one is small, the large strain invariant fit is used. The code switches smoothly between the two segments automatically.

Table A.1. Coefficients for Slip-Tube Strain Energy as a Power Series in Strain Invariants

Constant	$I_1 \le 5.0$ and $I_2 \le 6.27$	$I_1 \le 10.0$ and $I_2 \le 12.0$
c00	0	0
c10	0.0851661	0.0943634
c01	0.057562	0.043431
c11	-0.00334862	0.00113886
c20	-0.00478368	-0.00745304
c02	-0.00280587	-0.000935738
c21	-0.000418954	-0.000340933
c12	0.000503024	0.0000767233
c30	0.000841539	0.000553051

c03	0.000609627	-0.0000339206

The stress in principal stretch direction α is

$$\frac{\sigma_\alpha^{ST}\det(\underline{\underline{\lambda}})}{G_e} = 2\lambda_\alpha^2 c_{10} + 2\lambda_\alpha^2 c_{01} B + 2\lambda_\alpha^2 c_{11}\left[(I_2-3)+B(I_1-3)\right] + 4\lambda_\alpha^2 c_{20}(I_1-3) + 4\lambda_\alpha^2 c_{02} B(I_2-3) + 2\lambda_\alpha^2 c_{21}\left[2(I_1-3)(I_2-3)+B(I_1-3)^2\right] + 2\lambda_\alpha^2 c_{12}\left[(I_2-3)^2+2B(I_1-3)(I_2-3)\right] + 6\lambda_\alpha^2 c_{30}(I_1-3)^2 + 6\lambda_\alpha^2 c_{03} B(I_2-3)^2 + p$$

(A.8)

where

$$B = \lambda_\beta^2 + \lambda_\gamma^2$$

(A.9)

This gives the total Cauchy stress for strain energy type 3 as

$$\underline{\underline{\sigma}} = \frac{G_e}{\det(\underline{\underline{\lambda}})}\underline{\underline{\sigma}}^{ST} - \underline{\underline{I}}\frac{Tr\left(\frac{G_e}{\det(\underline{\underline{\lambda}})}\underline{\underline{\sigma}}^{ST}\right)}{3} + \frac{G_e}{G}\kappa\ln\left[\det(\underline{\underline{\lambda}})\right] + \sum_{i=1}^{nstages}\left\{\underline{\underline{\sigma}}_i^{affine} - \underline{\underline{I}}\frac{Tr\left(\underline{\underline{\sigma}}_i^{affine}\right)}{3} + \frac{G_i}{G}\kappa\ln\left[\frac{\det(\underline{\underline{\lambda}})}{\det(\underline{\underline{\lambda}}_i)}\right]\right\}$$

(A.10)

where again G_e is included in G if the first stage crosslinks are not in their state of ease. Similar to the Ogden model, only the initial gelation can trap entanglements, which causes the entanglements to have the original deformation as their state of ease.

A.3. Parameter Explanations

This section describes the parameters that must be given through the input deck. These parameters relate to the material model flory and do not include solver specific formulations. All these parameters should be entered in consistent units. Where appropriate, the parameters are identified with variables in the previous section.

A.3.1. Material Parameters

A.3.1.1. Physical Properties

The density of the material must be specified along with two of the six elastic constants. Generally, the Young's modulus and Poisson's ratio are specified. Since this is a model for

rubber, the Poisson's ratio should be close to 0.5. However, a value of exactly 0.5 will cause numerical error in calculating the other elastic constants. The shear and bulk moduli are calculated only once from the input Young's modulus and Poisson's ratio and, thus, remain constant through the calculation even as the material changes. This may cause some unexpected behavior in the convergence since an augmented Lagrangian approach is used with shear and bulk modulus scaling based on the initial values.

The number of reference states and their reference deformations are set using the state function. This should be a piecewise continuous function so that an integer is specified at every time. Care should be taken in setting reference states because the reference deformation is set on the first iteration of the given time. Thus, to get an equilibrated reference deformation, one should hold at the desired deformation for an extra time step and set the new reference state during the extra time step. Reference states should be set for any chemical changes (e.g., scission occurs, but not crosslinking) and the corresponding crosslink densities set accordingly. A crosslink density must be set for every reference state even if no crosslinks were introduced in that state. In addition, the number of reference states is a cumulative total, so even if all crosslinks are removed from some network, the reference state must remain with crosslink density set to zero.

A.3.1.2 Chemical Properties

The cross X functions are used to specify G_i for use in Eqs. A.1, A.2, A.4, and A.10. X refers to the reference state in which the crosslinks were inserted. The values should be input as

$$\text{cross X function} = \frac{\text{number of stage X crosslinks remaining} * \text{R} * \text{temperature}}{\text{original volume}} \tag{A.11}$$

where R is the gas constant in units that will cause cross X function to have units of pressure matching the elastic constants. Notice that this is a crosslink density. The stress calculation assumes a tetrafunctional network with the affine model having twice as many strands as crosslinks (G_i=2*cross X function) and the phantom model having the number of strands equal to the number of crosslinks (G_i=cross X function). In principal, any functionality can be used simply by adjusting the cross X function to account for the translation between cross X function and G_i.

For the entanglement contributions, the entden tX functions work similarly to the cross X function except that the reference state is always the original deformation. However, the analogous expression

$$\text{entden tX function} = \frac{\text{number of entanglements} * R * \text{temperature}}{\text{original volume}}$$

(A.12)

is not quite correct. If a_2 is negative in Eq. A.3, then the entden t2 function must also be negative. The exponents a_1 and a_2 for Eq. A.3 are given using the entexp tX functions where X is 1 or 2.

For the slip-tube model, the entden t1 function is used to calculate G_e in Eq. A.10. In their original formulation of the slip-tube model, Rubinstein and Panyukov effectively set

$$G_e = \frac{4}{7} * \frac{\text{number of monomers}}{\text{N}_\text{e} * \text{original volume}}$$

(A.13)

where N_e is the number of monomers between entanglements. The program corrects for this oddity by multiplying the given value for entden t1 function by 7/4 so that the G_e used in the calculation matches the idea that G_e is the plateau modulus from shear experiments that is retained by trapping the entanglements.

The flag "phi onoff" controls whether the stress transfer functions are used. A value of one will cause the program to calculate and use stress transfer functions. A value of zero prevents the use of stress transfer functions. The generalized stress transfer functions from the Fricker formula[v] are

$$\Phi_x^{Rj} = \frac{\text{stage x crosslinks removed in stage j}}{\text{total number of crosslinks added (up through stage j)}} = \frac{G_x^{Rj}}{\sum_{k=1}^{j} G_k^*}$$

(A.14)

where G_k^* is the initial modulus for the network formed in stage k, G_x^{Rj} is the difference between the modulus of the stage x network at the beginning of stage j and at the end of stage j (i.e., the effect of the scissions for the stage x networks that occur during stage j), and Φ_x^{Rj} is the stress transfer function for the stage i network based on chemical changes during stage j.

The effective modulus (G_p^{eff}) for each stage p of the total n stages is calculated from

$$G_p^{eff} = G_p\left(1 - \sum_{i=1}^{p-1}\sum_{k=p}^{n} \Phi_i^{Rk}\right) + \sum_{i=p+1}^{n} \Phi_p^{Ri} \sum_{k=p+1}^{i} G_k$$

(A.15)

where G_x is the current modulus for the network formed at stage x. For notational convenience, if the end index is smaller than the start index, no terms are summed. Notice that this formulation assumes an isothermal process. Note also that entanglements are not included in stress transfer functions.

A.3.2. Numerical Parameters

The flag "strain energy type" can have three values: 1 denotes affine model, 2 denotes affine model with Ogden entanglements, and 3 denotes phantom model with slip-tube entanglements. All three types can have the "phi onoff" flag set to either on (1) or off (0).

The value of "tol function" indicates a threshold for a deviation from unity. If the value of "tol function" is greater than the value of $\ln\left[\frac{\det \underline{\underline{\lambda}}}{\det \underline{\underline{\lambda}}_{ref}}\right]$, then $\left[\frac{\det \underline{\underline{\lambda}}}{\det \underline{\underline{\lambda}}_{ref}}\right]$ is considered unity. No default exists for "tol function"; the recommended value is 1.0×10^{-6}.

This model is configured to work with an augmented Lagrangian solution method. Thus, an adagio multilevel solver block with a control stiffness block should be used. In addition, the parameters for material model flory block must contain "reference strain", "max poissons ratio" (ν_{max}), and "target E" (E_{tar}). Generally, "reference strain" = -1. The other two parameters are used to set the bulk and shear scaling for the augmented Lagrangian technique. The scaling factors are calculated as

$$2G_{real} = 4\sum_{X=1}^{5} crossXfunction(t=0)$$

(A.16)

$$2G_{scaled} = \frac{E_{tar}}{1+\nu_{\max}}$$

(A.17)

$$SCALE_{2G} = \frac{2G_{scaled}}{2G_{real}}$$

(A.18)

$$\kappa_{scaled} = \frac{2G_{scaled} * (1+\nu_{\max})}{3*(1-2\nu_{\max})}$$

(A.19)

$$SCALE_{\kappa} = \frac{\kappa_{scaled}}{\kappa}$$

(A.20)

$SCALE_{2G}$ has a minimum value of unity, while $SCALE_{\kappa}$ has a maximum value of unity.

Table A.2. Summary of Parameters for Property Specification for Material Model Flory

Entry	Description
cross X function	Real function of time. These functions are used to set the modulus for the crosslinks. Five terms (X=1 to 5) should be given even if some need to be set to zero. Should have pressure units.
entden tX function	Real function of time. Used to set entanglement moduli for strain energy types 2 and 3. However, both terms (X=1 and 2) must be set for all systems even if not used. Zero is an acceptable value function. Should have pressure units.
entexp tX function	Real function of time. Used to set the exponents for the Ogden entanglement terms. However, both terms (X=1 and 2) must be set for all systems even if not used. Zero is an acceptable function.
max poissons ratio	Real, constant used as Poisson's ratio to set the scaling for the augmented Lagrangian technique. Should be between 0 and 0.5.
phi onoff	integer flag for stress transfer functions 1=calculate and use 0= neglect them
reference strain	Real, constant used for the augmented Lagrangian technique. Usually set to -1.
state function	integer function of time indicating a running total of reference states This function must be constant or piecewise continuous.
strain energy type	integer flag indicating 1=affine model (crosslinks only) 2=affine model with Ogden entanglements 3=phantom model with slip-tube entanglements
target E	Real, constant used as Young's modulus to set the scaling for the augmented Lagrangian technique. Should have pressure units.
tol function	real function of time that indicates a threshold for deviations from reference states. If $\ln\left\lfloor \frac{\det \underline{\underline{\lambda}}}{\det \underline{\underline{\lambda}}_{ref}} \right\rfloor$ is greater than tol function, the system is away from its reference state.

A.4. References

i. R.D. Andrews, A. V. Tobolsky, and E. E. Hanson "The Theory of Permanent Set at Elevated Temperatures in Natural and Synthetic Rubber Vulcanizates" J. Appl. Phys. **17**, 352 (1946).
ii. R. W. Ogden *Non-linear Elastic Deformations* Dover, Mineola, N.Y. (1997), p.221.
iii. N. R. Langley and K. E. Polmanteer "Relation of Elastic Modulus to Crosslink and Entanglement Concentrations in Rubber Networks" J. Polym. Sci.: Polym. Phys. Ed. **12**, 1023 (1974).
iv. M. Rubinstein and S. Panyukov "Elasticity of Polymer Networks" Macromolecules **35**, 6670 (2002).
v. H. S. Fricker "The Effects on Rubber Elasticity of the Addition and Scission of Cross-links under Strain" Proc. Roy. Soc. London Ser. A Math Phys Sci **335**, 267 (1973).

APPENDIX B: FORTRAN PROGRAM FOR CALCULATING g_α

```
      program rpscale
c     Description:
c           This program will calculate the scaling factors(g) for use
c           with the slip-tube model of Rubinstein-Panyukov
c           Macromolecules 35, 6670 (2002)
c     The main program is a driver to give a set of stretch ratios and
c     receive the corresponding scaling factors (sqrtg).
c     This driver calculates a set of stretches by looping over stretch
c     1 and stretch 2 and calculating stretch 3 using incompressibility
c     Since this is an iterative process, the oldscale for the next
c     combination of stretches is the current scale times 0.80.

c     Variables:
c           i             int     loop variable
c           j             int     loop variable
c           k             int     loop variable
c           maxlambda?    int     maximum number of times to change
c                                 the stretch in the ? direction
c                                 maxlambda1 controls the outer
c                                 stretch(1) loop while maxlambda2
c                                 controls the inner stretch(2) loop
c           oldscale      real    sqrtg in three directions as an
c                                 initial guess
c           one           dp      1.0d0
c           scale         real    sqrtg in three directions as current
c                                 result
c           steplambda    real    an increment to increase or decrease
c                                 stretches 1 and 2
c           stretch real  principal stretches in 3 directions
c
c     Subroutines:
c           secant: uses a secant method to solve for sqrtg(2)
c
c     Output files:
c           sqrtg.out: contains the three stretches and three sqrtg
c
c
c*************************************************************************
      implicit none
      real stretch(3),scale(3),oldscale(3),steplambda
      parameter(steplambda=0.05)
      double precision one
      parameter(one=1.0d0)
```

```
      integer i,j,k,maxlambda2,maxlambda1
      parameter(maxlambda1=2,maxlambda2=11)

      open(10,file="sqrtg.out")
      write(10,*) "stretch1 stretch2 stretch3 sqrtg1 sqrtg2 sqrtg3"

      oldscale(1)=1.294
      oldscale(2)=1.03
      oldscale(3)=0.51
      scale(1)=1.298
      scale(2)=1.02
      scale(3)=0.52
      stretch(1)=2.5
      stretch(2)=1.2

      do 500 k=1,maxlambda1
        stretch(1)=stretch(1)-steplambda
        stretch(2)=1.2
        do 100 i=1,maxlambda2
          stretch(2)=stretch(2)-steplambda
          stretch(3)=one/(stretch(2)*stretch(1))
          call secant(oldscale,stretch,scale)
          write(10,*) stretch,scale
          do 10 j=1,3
            oldscale(j)=0.80*scale(j)
10        continue
100     continue
500   continue
      stop
      end


**********************************************************************
      subroutine secant(oldscale,stretch,scale)
c**********************************************************************
c     Description:
c           This subroutine uses the secant method to solve
c           for three scaling factors, given three principal
c           stretches and initial guesses.
c           The equation I need to solve is
c           G=sum(g(i))-3=0
c
c           E. Kreyszig Advanced Engineering Mathematics 8th ed
c                 John Wiley & Sons NY (1999) p. 846 details the
c                 secant method
c
```

```
c               The secant method will give me
c               x(n+1)=x(n)-G(x(n))*{x(n)-x(n-1)}
c                                 /{G(x(n))-G(x(n-1))}
c               x is the scale factor (sqrtg) for direction = 2
c                       (an arbitrary choice).

c
c       Variables:
c               anumerator      real    numerator for equation to solve
c                                               secant method
c                                       (gbeta(n)-gbeta(n-1))
c               bigG            real    sum of squares of current scaling
c                                        factors
c               denominator     real    denominator for equation to solve
c                                               secant method
c                                       (G(sqrtg(2,n)-G(sqrtg(2,n-1))
c               i               int     loop index
c               maxiter         int     maximum number of iterations to
c                                               attempt
c               oldbigG         real    bigG from last iteration
c               oldscale        real    scaling factors (sqrtg) from
c                                       the last iteration
c               outerloop       int     loop index for the overall method
c               scale           real    current values of the scaling factors
c                                               (sqrt(g))
c               stretch real    principal stretches
c               three           real    3.0d0
c               tol             real    tolerance to determine when to
c                                       stop iterating.  Both numerator
c                                       and denominator are compared to it.
c               zero            real    0.0d0
c
c       Subroutines:
c               cubicsolve: returns the physical root of the cubic
c                               equation.  This returned value is sqrt(g).
c**********************************************************************
        implicit none
        integer i,outerloop,maxiter
        parameter(maxiter=100)
        real anumerator,denominator,tol
        parameter(tol=1.0e-09)
        real stretch(3),scale(3),oldscale(3),bigG,oldbigG
        real zero,three
        parameter(zero=0.0d0,three=3.0d0)

        oldbigG=-3
```

```
      do 10 i=1,3
            oldbigG=oldbigG+oldscale(i)*oldscale(i)
10    continue

      do 100 outerloop=1,maxiter

c     calculate the new scale values
       call cubicsolve(stretch(2),scale(2),stretch(1),scale(1))
       call cubicsolve(stretch(2),scale(2),stretch(3),scale(3))

c     calculate new bigG
       bigG=-3
       do 20 i=1,3
            bigG=bigG+scale(i)*scale(i)
20     continue

c     apply the secant calculation
       anumerator=scale(2)-oldscale(2)
       denominator=bigG-oldbigG

c     Check for convergence and ensure not to divide by zero
       if(abs(denominator).le.tol.or.abs(anumerator).le.tol) then
c     this exit is a Fortran 90 command to break the do loop
            exit
       endif

       oldscale(2)=scale(2)
       scale(2)=oldscale(2)-bigG*anumerator/denominator
       oldbigG=bigG

100   continue

      return
      end


c**********************************************************************
      subroutine cubicsolve(sbeta,gbeta,salpha,galpha)
c**********************************************************************
c     Description:
c       This subroutine will solve the cubic equation associated with
c       using the Lagrangian multiplier.
c     I am solving for galpha, given sbeta, gbeta, salpha
c
c     The Lagrangian multiplier equation is (see Book7, p47)
c            12/A*bigLambda=-3*sbeta/gbeta**3+3/(gbeta*sbeta)
```

```
c                                   -4/(gbeta*gbeta)
c             where A is the prefactor containing chain density, kT, and
c             imaginary chain length.  I don't need to calculate it here
c             because it cancels.
c
c       Thus, the governing cubic equation is
c       bigZ*galpha**3+bigC*galpha**2+bigD*galpha+bigE=0
c             bigZ=bigLambda*12/A*salpha
c             bigC=-3
c             bigD=4*salpha
c             bigE=3*salpha**2
c
c       A cubic equation gives
c             y**3+p*y**2+q*y+r=0
c             p=bigC/bigZ
c             q=bigD/bigZ
c             r=bigE/bigZ
c
c       Numerical Recipes recommends testing
c             Q=(p**2-3*q)/9
c             R=(2*p**3-9*p*q+27*r)/54
c       Two cases exist.
c             If R^2<Q^3, three real roots exist
c                   theta=arccos(R/sqrt(Q^3))
c                   y1=-2*sqrt(Q)*cos(theta/3)-p/3
c                   y2=-2*sqrt(Q)*cos((theta+2pi)/3)-p/3
c                   y3=-2*sqrt(Q)*cos((theta-2pi)/3)-p/3
c             If R^2>=Q^3, only one real root exists
c                   A=-{R+sqrt(R^2-Q^3)}^(1/3)
c                   B=Q/A (or zero if A=0)
c                   y=A+B-p/3
c
c       For more than one root, I check to ensure that the root squared
c  is between 0 and 3.  If more than one root meets this test, the last
c  root found will be returned to the calling program.

c       Variables:
c       Note: most of the variables are short-hand terms to substitute in
c       the equation.  Those variables are defined in the Description
c       section.
c
c             four    dp      4.0d0
c             galpha  real    RP scaling factor in the alpha direction
c                              (this really is sqrt(galpha) in the RP
c                                    equation)
c             gbeta   real RP scaling factor in the beta direction
```

```
c                              (this really is sqrt(gbeta) in the RP
c                                    equation)
c               i       int    loop index
c               icount  int    checks if more than one root was between
c                                    0 and 3.
c               isign   int    a placeholder so that I can take the cube
c                              root of a negative number
c               one     dp     1.0d0
c               sbeta   real   beta direction stretch
c               salpha  real   alpha direction stretch
c               three   dp     3.0d0
c               two     dp     2.0d0
c               twopi   real   2*pi
c               x       real   array to hold multiple roots
c               zero    dp     0.0d0
c*************************************************************************
      implicit none
      double precision three,four,one,two,zero
      parameter(three=3.0d0,four=4.0d0,one=1.0d0,two=2.0d0,zero=0.0d0)
      real bigA,bigB,bigC,bigD,bigE,bigZ,bigLambda,bigQ,bigR
      real p,q,r
      real sbeta,gbeta,salpha,galpha,x(3),twopi,theta
      parameter(twopi=6.283184)
      integer i,icount,isign
      icount=0

      bigLambda=-three*sbeta/(gbeta**three)
     &     +three/(gbeta*sbeta)-four/(gbeta*gbeta)
      bigZ=bigLambda*salpha
      bigC=-three
      bigD=four*salpha
      bigE=three*salpha*salpha

      p=bigC/bigZ
      q=bigD/bigZ
      r=bigE/bigZ


      bigQ=(p*p-three*q)/(three*three)
      bigR=(two*p*p*p-three*three*p*q+three**three*r)/
     &(three*three*three*two)

c     Check for the possibility of three real roots
      if(bigQ**three.gt.bigR**2) then
            theta=acos(bigR/sqrt(bigQ**3))
            x(1)=-two*sqrt(bigQ)*cos(theta/three)-p/three
```

```
            x(2)=-two*sqrt(bigQ)*cos((theta+twopi)/three)-p/three
            x(3)=-two*sqrt(bigQ)*cos((theta-twopi)/three)-p/three

c       Now I need to find the physical root
            do 10 i=1,3
                  if(x(i).gt.zero.and.(x(i)*x(i)).lt.three)
     &      then
                        icount=icount+1
                        galpha=x(i)
                  endif
 10         continue
        else
            isign=1

            bigA=sqrt(bigR*bigR-bigQ*bigQ*bigQ)
            bigA=bigA+bigR

c       Hold a negative number in isign so that I can take the cube root
c       of a negative number
            if(bigA.lt.zero) isign=-1
            bigA=abs(bigA)**(one/three)
            bigA=float(isign)*bigA
            bigA=-bigA
            if(bigA.ne.zero) then
                  bigB=bigQ/bigA
            else
                  bigB=zero
            endif
            galpha=bigA+bigB-p/three
        endif

        return
        end
```

DISTRIBUTION

1	MS0139	Paul Yarrington	1902
1	MS0139	Robert K. Thomas	1904
1	MS0321	Jennifer E. Nelson	1430
1	MS0372	Chi S. Lo	1524
1	MS0372	John Pott	1524
1	MS0557	Daniel Segalman	1525
1	MS0847	Peter J. Wilson	1520
1	MS0885	Justine Johannes	1810
1	MS0885	Richard Salzbrenner	1820
1	MS0887	Duane Dimos	1800
1	MS0888	Doug Adolf	1821
1	MS0888	Robert Bernstein	1821
1	MS0888	Roger Clough	1821
1	MS0888	Robert Chambers	1526
1	MS1303	Gary Grest	1114
1	MS1322	John Aidun	1435
1	MS1322	Aidan Thompson	1435
1	MS1349	John Curro	1815
1	MS1349	Dana Rottach	1815
1	MS1411	Roger Assink	1821
5	MS1411	Joanne Budzien	1814
1	MS1411	Mat Celina	1821
1	MS1411	H. Eliot Fang	1814
1	MS1411	Ken Gillen	1821
1	MS1415	Carlos Gutierrez	1114
1	MS9404	Davina M. Kwon	8770
1	MS9042	Vera Revelli	8774
1	MS9403	Linda Domeier	8778
2	MS9018	Central Technical Files	8944
2	MS0899	Technical Library	4536